

Difficulties of Quantitative Tests of the Kerr-Hypothesis with X-Ray Observations of Mass Accreting Black Holes

Henric Krawczynski

Printed: July 26, 2018

Abstract X-ray studies of stellar mass black holes in X-ray binaries and mass-accreting supermassive black holes in Active Galactic Nuclei have achieved a high degree of maturity and have delivered detailed information about the astrophysical sources and the physics of black hole accretion. In this article, I review recent progress made towards using the X-ray observations for testing the “Kerr hypothesis” that the background spacetimes of all astrophysical quasi-stationary black holes are described by the Kerr metric. Although the observations have indeed revealed clear evidence for relativistic effects in strong-field gravity, quantitative tests of the Kerr hypothesis still struggle with theoretical and practical difficulties. In this article, I describe several recently introduced test metrics and review the status of constraining the background spacetimes of mass accreting stellar mass and supermassive black holes with these test metrics. The main conclusion of the discussion is that astrophysical uncertainties are large compared to the rather small observational differences between the Kerr and non-Kerr metrics precluding quantitative constraints on deviations from the Kerr metric at this point in time. I conclude with discussing future progress enabled by more detailed numerical simulations and by future X-ray spectroscopy, timing, polarimetry, and interferometry missions.

Keywords General Relativity · Black Holes · No-Hair Theorem · Kerr Hypothesis · Black Hole Spins

PACS PACS 95.30.Sf · PACS 97.60.Lf

H. Krawczynski
Physics Department and the McDonnell Center for the Space Sciences Washington University in Saint Louis 1 Brookings Dr., CB 1105 Saint Louis, MO 63130
Tel.: +314-935-8553
E-mail: krawcz@wustl.edu

1 Introduction

General Relativity’s (GR’s) no-hair theorem states that the Kerr [94, 178] and Kerr-Newman [133, 132] families of background spacetimes are the only stationary, axially symmetric, and asymptotically flat vacuum (Kerr) and electro-vacuum (Kerr-Newman) solutions of the Einstein equations that have an event horizon and neither singularities nor closed timelike curves in the outer domain [83]. As astrophysical black holes are thought to be largely electrically neutral [25, 181], the no-hair theorem implies the “Kerr hypothesis” that if GR and the assumptions made for deriving the no-hair theorem are valid, the background spacetimes of all quasi-stationary astrophysical black holes can be described by the Kerr family of metrics. If the Kerr hypothesis holds, astrophysical black holes are as simple as elementary particles. Of course, tests of the Kerr hypothesis only depend on the spacetime geometry of black holes, and do not test the dynamical aspects of the underlying theory.

The present article follows several excellent reviews of tests of GR in the weak and strong gravity regimes and tests of the Kerr hypothesis. In his review “The Confrontation between General Relativity and Experiment”, Will posits that the tests of Einstein’s equivalence principle (the trajectories of freely falling bodies do not depend on their structure and composition plus local Lorentz and position invariance) with exquisite accuracy strongly argue for gravity being described by a metric theory [192]. After reviewing theoretical frameworks for testing GR such as the Parametrized Post Newtonian (PPN) formalism, he gives a broad overview of alternative theories of gravity including scalar tensor theories, $f(R)$ theories, vector tensor theories, tensor-vector-scalar theories, quadratic gravity, and massive graviton theories. He summarizes the state of the art

of GR's validation based on solar system and stellar system observations, and outlines the potential of gravitational wave detections.

In the review article “Probes and Tests of Strong-Field Gravity with Observations in the Electromagnetic Spectrum” Psaltis argues for the need of testing GR in the strong-gravity regime [145]. He characterizes the strength of the gravitational field of an object of mass M at a distance r with the depth of the potential well $\varepsilon = GM/r c^2$ and the spacetime curvature $\xi = GM/r^3 c^2$. Observations of phenomena close to event horizons of rapidly spinning stellar mass black holes test GR at ~ 10 orders of magnitude larger ε -values and ~ 5 orders of magnitude larger ξ -values than solar system tests and observations of the Hulse-Taylor binary pulsar. Psaltis describes different observational channels for GR tests, i.e. electromagnetic observations of inspiralling compact binaries, Very Long Baseline Interferometric observations of the shadows of the black holes in Sgr A* and M 87, X-ray evidence for the existence of stellar mass black holes, lines in the X-ray energy spectra of black holes and neutron stars, black hole size constraints from X-ray timing observations, and the analysis of the quasi-periodic oscillations of the X-ray fluxes from mass accreting neutron stars and black holes.

The three reviews “Gravitational-Wave Tests of General Relativity with Ground-Based Detectors and Pulsar-Timing Arrays” by Yunes & Siemens [196], “Testing general relativity with present and future astrophysical observations” by Berti et al. [22], and “Testing General Relativity with Low-Frequency, Space-Based Gravitational-Wave Detectors” by Gair, Vallisneri, Larson, and Baker [62] follow up on Will's review. The authors give an expanded review of alternative theories of gravity and discuss the existence and properties of compact objects and gravitational waves in these theories. The interested reader is referred to Tables 1-3 of Berti et al.'s paper for summaries of alternative theories of gravity and how they relate to the assumptions of Lovelock's theorem (Table 1), and the properties of black holes (Table 2) and neutron stars (Table 3) in these theories. The three reviews summarize strong-field tests of GR based on gravitational wave detections. Yunes & Siemens formulate criteria which make an alternative theory of gravity a well motivated and useful tool for strong-field tests of GR: a theory should be motivated from a fundamental physics standpoint, predictive for a range of initial value data, consistent with all current tests of GR, and should make strong-field predictions deviating from GR. They conclude that most alternative theories of gravity fail to meet one or several of these criteria with the exception of scalar-tensor

theories with spontaneous scalarization which meet the first three criteria and possibly the fourth criterion.

The two reviews “Testing the no-hair theorem with observations of black holes in the electromagnetic spectrum” by Johannsen [93] and “Testing black hole candidates with electromagnetic radiation” by Bambi, Jiang, and Steiner [18] are closely related to this paper. Both papers discuss tests of the Kerr hypothesis using parametric test metrics, and present predicted observational results for a range of different parameter values. Johannsen's review includes a detailed description of the status of testing the Kerr hypothesis with radio interferometric observations of the black hole shadows of Sgr A* and M 87, and stars orbiting Sgr A*. Compared to these earlier reviews, I will emphasize in this paper that X-ray tests of the Kerr hypothesis are currently of limited value owing to large systematic uncertainties stemming from astrophysical uncertainties and from modeling the systems with restrictive assumptions and limited fidelity.

Following Will's rationale, we will focus the discussion in this paper on tests of GR versus other metric theories of gravity in which the gravitational effects are fully described by the metric, the law of energy-momentum conservation holds (i.e. the covariant derivative of the energy-momentum tensor vanishes: $\nabla \cdot \mathbf{T} = 0$), and photons and massive particle follow geodesics of the metric. In the case of theories that can be derived from extremizing an action, the law of energy-momentum conservation can be derived from the requirement of the diffeomorphism invariance of the action as long as there is a separation of the matter and field actions (see [31] and also [56, 180, 169]). Electromagnetic tests of the Kerr hypothesis then involve the comparison of predictions derived for the Kerr spacetime and alternative spacetimes. The latter may result from alternative theories of gravity, or may be of purely phenomenological nature. In both cases, the metrics depend not only on a mass and an angular momentum parameter, but also on additional deviation parameters. All the metrics considered in the following include the Kerr family of metrics for certain values of the deviation parameters (i.e. 0 for additive terms, or 1 for multiplicative terms). Unfortunately, strong gravity tests lack a canonical parameterization similar to the PPN parameterization used for testing GR in the weak-field and slow-motion limit [192, 144]. For many alternative theories of gravity it is not known if black hole solutions exist. If they do, the metrics have only been derived in the limit of low spin values with the exception of Einstein-Gauss-Bonnet-Dilaton gravity for which a high-spin metric has been derived numerically [97].

The rest of the paper is structured as follows. I start with a brief description of some of the key properties of accretion disks and coronas of mass accreting stellar mass and supermassive black holes in Sect. 2. After introducing several test metrics in Sect. 3, I discuss some of the physical properties of the spacetimes they describe in Sect. 4. Subsequently, I discuss the two main methods that are being used to constrain the properties of the background spacetimes of astrophysical black holes in Sect. 5 and summarize the results obtained for stellar mass black holes. The results confirm key GR predictions, i.e. that matter can orbit a black hole close to its event horizon emitting radiation with large gravitational and Doppler frequency shifts in agreement with the GR predictions. However, systematic uncertainties are still too large to allow for robust tests of the Kerr metric against other metrics. I summarize my conclusions in Sect. 6, and discuss avenues for future progress.

Most of the reviews mentioned above were written before the detection of gravitational waves from the binary stellar mass black hole mergers GW150914 [1], GW151226 [3], GW170104 [4], GW170608 [5], and GW170814 [6] and the binary neutron star merger GW170817 [7]. The discoveries by LIGO and now also by VIRGO and the radio to gamma-ray observations of the electromagnetic counterpart of GW170817 have already led to important tests of GR and fundamental physics. The results include the test of GR's prediction that gravitational waves and gamma-rays propagate with the same speed with an accuracy of a few parts in 10^{15} [109], the confirmation that the spacetime curvature generated by the Milky Way affects gravitational waves and gamma-rays in the same way within an accuracy of a few parts in 10^6 [109], and the test of GR's prediction of two spin-2 tensor polarizations of gravitational waves [6]. The gravitational wave event GW150914 was used for parametric tests, i.e. constraints on higher-order post-Newtonian parameters and on GR deviation parameters of parametrized waveforms [2]. The results show the power of opening up a new observational window, and the fundamental physics insights that can be gained from observing dynamical gravity in action.

In the following we use the definition of the black hole region of an asymptotically flat spacetime being the region from which no future-pointing null geodesic can reach future null infinity. The event horizon (a null hypersurface in four dimensional spacetime) is defined as the boundary of this region. Throughout the paper, we use geometric units ($G=c=1$) and express all distances in units of the gravitational radius $r_g = GM/c^2$ with M being the black hole mass. Denoting the angular momentum by J , the spin parameter is given by

$a = J/cr_g M = cJ/GM^2$. In units of M , the spin parameter a can range from -1 to +1.

2 Black Hole Accretion Disks and Coronas

The theory of geometrically thin, optically thick accretion disks is based on the papers by Shakura & Sunyaev (1973) [166], Novikov & Thorne [135], and Page & Thorne [138]. The matter is assumed to orbit the black hole on near-Keplerian orbits in the equatorial plane of the spacetime. Turbulent viscosity described by the α -parameter transports angular momentum outwards enabling matter to flow inwards. The accreting matter is assumed to move from circular to circular orbit, locally emitting all the excess gravitational energy as it sinks towards the black hole. Assuming that the matter plunges into the black hole once it reaches the Innermost Stable Circular Orbit (ISCO) and the viscous torque vanishes at the ISCO, the conservation laws for mass, energy, and angular momentum fully determine the radial brightness distribution $F(r)$. The thin disk models are believed to hold for accretion luminosities $\dot{M}c^2$ (mass accretion rate times the speed of light squared) between a few percent and several ten percent of the Eddington Luminosity $L_{\text{Edd}} = 4\pi GMc/\kappa_{\text{es}}$ (with the electron scattering opacity being $\kappa_{\text{es}} \approx 0.4 \text{ cm}^2 \text{ g}^{-1}$). In this regime, the gravitational potential energy of the accreted mass is believed to be efficiently converted into radiation with an accretion efficiency $\eta \equiv L/\dot{M}c^2$ on the order of $\sim 10\%$ (L being the bolometric luminosity of the emission). At extremely low and extremely high accretion rates, the accretion efficiency η is likely to be much lower as the matter is either too tenuous to radiate efficiently for $L \ll L_{\text{Edd}}$ or advects diffusively trapped photons alongside the matter into the black hole for $L \geq L_{\text{Edd}}$. The magnetorotational instability (MRI) is believed to be the prime source of the viscosity driving the accretion [14]. Tests of the Kerr hypothesis are usually based on systems believed to accrete via geometrically thin and optically thick accretion disks. Descriptions of accretion flows in other regimes can be found in [9, 55].

General relativistic magnetohydrodynamical (GRMHD) and general relativistic radiation magnetohydrodynamic (GRRMHD) simulations make it now possible to perform ab-initio simulations of accretion flows. GRMHD simulations have largely confirmed the results of the analytical thin disk theory, showing that the radial brightness distribution matches that of the analytical models to good approximation, and the emission from within r_{ISCO} accounts for only a few percent of the total disk luminosity [134, 143]. Ongoing work includes studies of the transport of magnetic field

and angular momentum (e.g. [114,58]), line blanketing and thermal instabilities (e.g. [85,124]), radiation transport (e.g. [160]), the Comptonization of photons (e.g. [130]), and the impact of different ion and electron temperatures on the accretion in the low-luminosity regime (e.g. [159]). Some of the current GRRMHD developments parallel similar earlier developments in stellar radiation magnetohydrodynamics, see [33] for an introduction and review.

For thin disks and a given accretion rate \dot{M} in units of the Eddington luminosity L_{Edd} , the radiated luminosity scales as $L_{\text{bol}} \propto \dot{M}$ (see Equ. (20) below). The energy flux F per proper disk area scales as $F \propto L_{\text{bol}}/r_g^2 \propto \dot{M}^{-1}$, and the energy scale of the emitted photons scales with the photospheric temperature $T \propto F^{1/4} \propto \dot{M}^{-1/4}$ (see Equ. (22) below). Whereas the thermal disk emission of stellar mass black holes has keV energies and can readily be observed with X-ray telescopes, that of AGNs is in the blue and UV bands and is often masked by the emission from other components of the accretion flow. The good agreement of Shakura, Sunyaev, Novikorn, and Thorne's analytical thin disk model with the results of numerical simulations explain its continued use more than four decades after its invention. The model can explain the observed X-ray energy spectra of the thermal state of accreting stellar mass black holes such as LMC X-3 [172], and the blue bumps in the spectral energy distributions (SEDs) of active galactic nuclei (AGNs) [49]. Some observations are not yet unambiguously explained, or seem to be in tension with thin disk theory. For example, optical microlensing observations of gravitationally lensed quasars [126], photometric quasar variability studies [86], and optical reverberation observations [48] all indicate that optical accretion disks are by a factor of ~ 2 larger than predicted by thin disk theory (see [77] for a possible explanation).

For both types of black holes, mass accreting stellar mass and supermassive black holes, a corona of hot plasma is believed to emit X-rays with a power law energy spectrum. Some of the X-rays irradiate the accretion disk prompting the emission of Fe K α fluorescent emission at plasma frame energies around 6.4 keV and reflected Compton hump emission (Fig. 1, see the *NuSTAR* results for Cyg X-1 for exemplary energy spectra [182]). The shape and location of the corona is still a matter of debate (see e.g. [70]). For AGNs, the shape of the relativistically broadened Fe K α line [193,52,39] and time lags inferred from the Fe K α -power law continuum cross correlation function [184] hint at very compact coronas very close (within a few r_g) to the black holes. Additional evidence for compact coronas comes from the amplitude of the brightness fluctuations

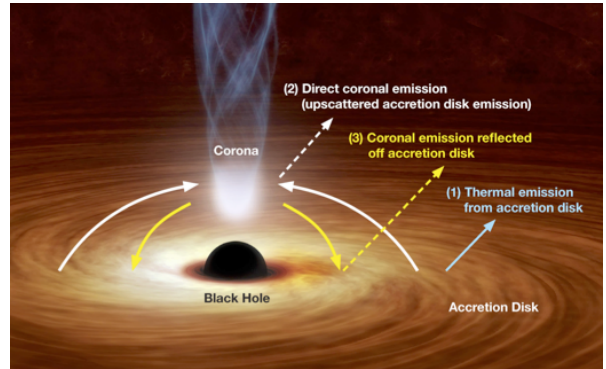


Fig. 1 Artist's impression showing (1) the thermal emission from the accretion disk, (2) the coronal emission, and (3) the reflected and reprocessed coronal emission (courtesy of JPL/NASA).

of the X-ray emission from gravitationally microlensed quasars (see Sect. 6).

X-ray astronomers often assume that the corona has a negligible spatial extent and is located on the rotation axis of the black hole and thus irradiates the accretion disk in a lamppost configuration [116]. GRMHD simulations indicate that such a configuration may arise from hot magnetized plasma rising buoyantly towards the underdense polar regions above and below the black hole [165]. Alternatively, the corona may be related to the launching site of a jet. Symmetry considerations argue for the existence of two of such coronas, one in each hemisphere of the black hole. For mass accreting supermassive black holes, there is some tension between the corona being sufficiently small to account for the results from gravitational lensing, spectroscopic and timing studies, and being sufficiently large to explain the observed X-ray fluxes via the Comptonization of accretion disk photons passing through the corona [46]. Current state-of-the-art models usually assume that the photosphere of the entire accretion disk can be described with a constant ionization parameter and a constant density of the accretion disk photosphere [156,64]. Eventually, more detailed numerical simulations should enable us to develop fitting models that account for the radial dependence of the ionization state and the density of the emitting plasma (see [65,183]).

3 Black Hole Test Metrics

Using the coordinates $x^\mu = (t, r, \theta, \phi)$, any stationary, axially symmetric and asymptotically flat metric can be brought into standard form:

$$ds^2 = -e^{-2\nu_0} dt^2 + e^{2\psi} (d\phi - \omega dt)^2 + e^{2\mu_1} dr^2 + e^{2\mu_2} d\theta^2 \quad (1)$$

with ν_0 , ψ , ω , μ_1 , and μ_2 being functions of r and θ only [34]. Assuming invariance under simultaneous inversion of t and ϕ , $\mu_1 = \mu_2$ already covers all possible metrics, but not requiring this equality provides for advantageous gauge choices. Setting $M = 1$ for convenience, the Kerr metric is given in Boyer Lindquist coordinates by [27]:

$$e^{-2\nu_0} = \Sigma \Delta / A, \quad e^{2\psi} = \sin^2 \theta A / \Sigma$$

$$e^{2\mu_1} = \Sigma / \Delta, \quad e^{2\mu_2} = \Sigma$$

$$\omega = 2ar/A, \quad \Delta = r^2 - 2r + a^2,$$

$$\Sigma = r^2 + a^2 \cos^2 \theta, \quad A = (r^2 + a^2)^2 - a^2 \Delta \sin^2 \theta. \quad (2)$$

The desire to quantitatively test the Kerr hypothesis has led to the development of a number of parametric test metrics. For the purpose of this paper, a test metric m is a map of N real parameters (a_1, a_2, \dots, a_N) to stationary, axially symmetric, asymptotically flat black hole metrics $g(a_1, a_2, \dots, a_N)$. A particular metric g is a black hole metric if the spacetime possesses an event horizon and no “pathologies”, i.e. neither curvature singularities at and outside of the event horizon, nor violations of the Lorentzian signature $\det(g) < 0$ or closed timelike curves outside of the event horizon. The metrics g may or may not be solutions of a field equation. A test metric is particularly useful if it satisfies a number of criteria:

- C1*: The range of the map $R(m)$ includes the Kerr family of metrics.
- C2*: $R(m)$ includes at least one valid black hole spacetime (i.e. a black hole spacetime without pathologies in the exterior domain) which is physically distinct from any Kerr spacetime.
- C3*: $R(m)$ covers a wide range of physically different black hole spacetimes.
- C4*: $R(m)$ includes the black hole metrics from one or several alternative theories of gravity such that observational constraints on the parameters a_1, a_2, \dots, a_N can be translated into constraints on the parameters of the alternative theories of gravity.
- C5*: The individual parameters of the test metric, or combinations of these parameters, can be identified with certain physical properties of the spacetimes.

In the remainder of this section, I discuss these criteria for a few metrics from the literature:

m1: Pani et al. (2011) derived slowly spinning black hole metrics for theories of gravity with an Einstein-Hilbert action augmented by quadratic and algebraic curvature invariants coupling to a single scalar field [139].

m2: Aliev and Gümrükçüoğlu (2005) argue that GR’s Kerr-Newman metric describes a black hole on a 3-brane in the Randall-Sundrum braneworld [12]. The Kerr-Newman charge parameter is interpreted to describe a “tidal charge”.

m3: Ghasemi-Nodehi & Bambi (2016) introduce 11 parameters modifying every occurrence of the mass parameter M and the spin parameter a in the Kerr metric, allowing them to modify how these two properties couple to the spacetime curvature [68].

m4: The Geroch-Hansen mass multipole moments M_l and current multipole moments S_l ($l \in \mathbb{N}_0$) of the Kerr metric depend only on two parameters M and a : $M_l^K + iS_l^K = M(ia)^l$ [67, 78, 57]. Glampedakis and Babak (2006) introduce a test metric by modifying the quadrupole moment with the help of a dimensionless deviation parameter ε : $M_2 = M_2^K - \varepsilon M^3$ and neglecting deviations in all higher moments [71].

m5: Johannsen & Psaltis (2011) derive a test metric (called *m5a* in the following) by applying the Newman-Janis algorithm to a Schwarzschild metric with the (t, t) and (r, r) components modified by a multiplicative factor of $(1 + h(r))$ and expanding the real function $h(r)$ in powers of $1/r$ [87]. Cardoso, Pani & Rico (2014) derive a generalized version of this test metric (called *m5b* in the following) using a seed metric with different modifiers for the (t, t) and (r, r) elements of the Schwarzschild metric, doubling the number of free parameters [30].

m6: Johannsen (2013, 2016) constructs a test metric that leaves the Hamilton-Jacobi equations of a test particle separable [88, 93] (see also the earlier work of [187]). Johannsen’s metric allows for three constants of motion, two associated with the Killing vectors of the temporal and axial symmetries, plus one “Carter constant” following from the separability of the Hamilton-Jacobi equations. The metric uses one parameter β and four functions $A_1(r)$, $A_2(r)$, $A_5(r)$, and $f(r)$ to modify the (t, t) , (t, ϕ) , (r, r) , (θ, θ) and (ϕ, ϕ) components of the Kerr metric. Expanding $A_1(r)$, $A_2(r)$, $A_5(r)$ around 1 and $f(r)$ around 0 in powers of $1/r$ leads to a set of expansion coefficients called α_{1n} , α_{2n} , α_{5n} , and ϵ_n , respectively, with n designating the power of $1/r$.

The test metrics *m4*, *m5*, and *m6* use power series in $1/r$ which should converge for $r/M \gg 1$, but which do not necessarily converge in the regime $r/M \sim 1$ which is of particular interest for X-ray tests of the Kerr hypothesis. Konoplya, Rezzolla and Zhidenko performed detailed studies of the convergence of various parameterizations of generally axially symmetric test metrics. They find that a continued-fraction expansion in terms of a compactified radial coordinate and a Taylor ex-

pansion in terms of the cosine of the polar angle shows excellent convergence – at least in the equatorial plane [101].

A test metric with a range including the Kerr family of metrics (criterion *C1*) can be used to constrain deviations from GR. All metrics *m1*–*m6* satisfy this criterion. Criterion *C2* requires that the range of the test metric includes one or more non-Kerr spacetimes. In Section 4 we will discuss a prescription that can be used to show that a test metric indeed produces spacetimes that are physically different from any Kerr spacetime (accounting for the gauge freedom). In addition, criterion *C2* requires that the metrics are regular in the exterior domain, assuring that numerical simulations can be run for these spacetimes. We know that the test metrics *m2* and *m6* satisfy this criterion, and that the test metrics *m4* and *m5a* do not. The non-Kerr metrics of the test metric *m4* are known to exhibit pathologies in the exterior domain, and the non-Kerr metrics of the test metric *m5a* (and *m5b*) exhibit curvature singularities at the event horizon [90,30]. To my knowledge, the regularity of the metrics *m1* and *m3* has not yet been studied so far. Even if a test metric does not satisfy criterion *C2*, it can still be used as a tool to scrutinize observational data for deviations from the Kerr spacetimes by neglecting any radiation entering or coming from the affected portions of the spacetimes, see e.g. [87,102,79,93,18].

Criteria *C3* and *C4* concern the richness of the spacetimes of the test metric. One possible way of showing that a test metric covers a non-trivial set of physically different spacetimes (criterion *C3*) is to show that it includes known black hole solutions from one or several alternative theories of gravity (criterion *C4*). Cardoso, Pani and Rico (2014) show that the test metric *m5b* covers the non-spinning black holes of the Einstein-Dilaton-Gauss-Bonnet gravity, but that neither *m5a* nor *m5b* cover the spinning counterparts [30]. The test metric *m6* covers the Kerr-Newman, Bardeen and modified gravity black hole spacetimes. For small values of the deviation parameter, the metric captures the Einstein-Dilaton-Gauss-Bonnet and dynamical Chern-Simons black hole solutions valid up to linear order in the spin parameter [93]. Another way of assessing the richness of $R(m)$, is to evaluate the observational signatures for all the parameters of the metric, see Sect. 4.

Finally, one would wish that certain parameters of the test metric can be identified with certain physical properties of the spacetime (criterion *C5*). Ghasemi-Nodehi & Bambi systematically explore the effect of the 11 parameters of the test metric *m3* on the observed appearance of black hole shadows [68]. Similarly, Table 3 of Johansen (2016) shows the impact of the param-

eters of the test metrics *m5a* and *m6* on certain types of observations.

4 Observational Signatures

Combining the analytical models of the coronal or accretion disk emission described in Sect. 2 with 4-D ray tracing codes, predicted X-ray flux and polarization energy spectra, light curves, and images can be derived. Ray tracing schemes track photons from the observer to the black hole [146,15], from the accretion disk or corona to the observer [102,21], or make use of Cunningham’s transfer function formalism [18]. Such codes have been used to study the impact of the background spacetime on Fe $K\alpha$ line shapes (e.g. [146,16,92,79,18]), continuum energy spectra (e.g. [102,15,92,79,13]), polarization energy spectra (e.g. [102,79]), the shapes of black hole shadows (e.g. [102,91,79]), and Fe $K\alpha$ reverberation signatures (e.g. [79]). All these studies assume that the angular momentum vectors of the black holes and the accretion disks align.

Figure 2 shows that the parameter ϵ_3 of the test metric *m5a* has a strong impact on the predicted Fe $K\alpha$ inner disk reflection spectra (from [89]). However, in the same paper, the authors note that the predicted energy spectra agree surprisingly well when comparing Kerr and non-Kerr metrics giving identical r_{ISCO} -values (Fig. 3). We found a similar approximate degeneracy of the Kerr and non-Kerr metrics in terms of the predicted observational signatures for the metrics *m1*, *m2*, *m4*, and *m5a* as long as we compare metrics with identical or similar r_{ISCO} -values. Fig. 4 shows the predicted flux and polarization energy spectra of the thermal disk emission for Kerr and non-Kerr models giving the same r_{ISCO} -values (from [102], see also [79]). The results demonstrate that the Kerr metric and the *m5a* metrics produce almost indistinguishable observational signatures for a considerable fraction of the *m5a* parameter space, including nominal non-Kerr metrics with a non-vanishing deviation parameter ϵ_3 . Kong, Li, and Bambi (2014) explored the degeneracy of the Kerr and *m5a* metric with regards to observational signatures by fitting theoretical Fe $K\alpha$ inner disk reflection energy spectra with the energy spectra derived for *m5a* background spacetimes (Fig. 5). The results establish an equivalence class of metrics with a and ϵ_3 -combinations mapping to near-identical observational results. Although it seems likely that the observationally degenerate metrics have similar r_{ISCO} -values, the authors did not comment on this in their paper.

In summary, for large regions of the parameter space, the test metrics *m1*, *m2*, *m4*, and *m5a* predict almost identical observational signatures as suitably cho-

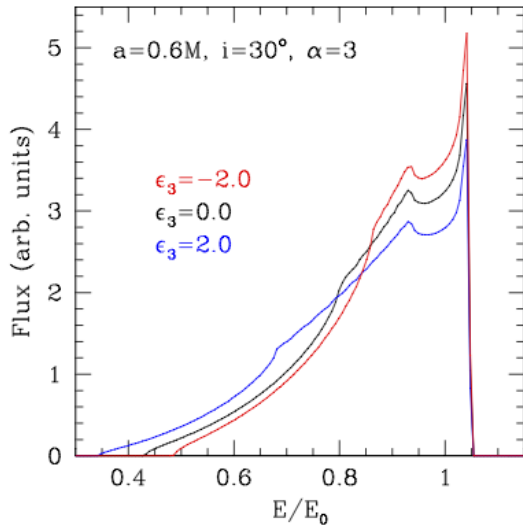


Fig. 2 Simulated Fe K α energy spectra for the test metric $m5a$ for $a = 0.6$, $i = 30^\circ$ for several values of the parameter ϵ_3 measuring the deviation from the Kerr metric. Reproduced from [89] with permission of the authors.

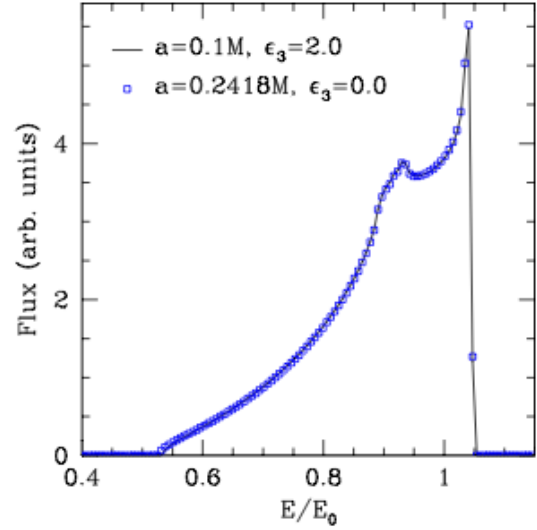


Fig. 3 Same as Figure 2 but for two combinations of spin parameter a and deviation parameter ϵ_3 giving the same r_{ISCO} -values. The two metrics lead to almost identical energy spectra (black solid line and blue squares). Reproduced from [89] with permission of the author.

sen Kerr metrics. The only exceptions seem to be spacetimes with r_{ISCO} -values larger than the maximum value $r_{\text{ISCO}} = 9$ for the Kerr spacetime. The results demonstrate the difficulty of evaluating the criteria $C2$ (the range of the metric includes one or more valid spacetimes which are physically distinct from the Kerr metric) and $C3$ (the test metric covers a rich range of physically different spacetimes) in the presence of degeneracies between the parameters of the test metric, and the gauge freedom of metric theories. One way of simplifying the analysis is to transition from using heavily degenerate metric parameters to parameters which are either related to observables or leave other observables unchanged. It is furthermore helpful to focus the discussion of the properties of a spacetime entirely on observables and to avoid using coordinates. In the remainder of this section, we demonstrate this procedure for the specific examples of the test metrics $m2$ and $m6$. The test metric $m2$ depends on the parameters M , a and β . For the test metric $m6$ we limit the discussion to the parameters M , a and α_{22} .

Rather than performing full ray tracing simulations, we use basic analytical equations to derive some pseudo-observables. We simplify the discussion of the physical properties of the spacetimes of the test metrics by using (M, P_{ISCO}, a) as the parameters characterizing a spacetime instead of (M, a, β) or (M, a, ϵ_3) . The parameter M describes for all metrics the mass measured by a distant observer, P_{ISCO} is the orbital period of matter orbiting the black hole at the ISCO as measured by a distant observer in the asymp-

totically flat region of the spacetime. The parameter a labels the one dimensional space of metrics with identical M and P_{ISCO} . The choice of comparing Kerr and non-Kerr metrics with the same P_{ISCO} with each other is not unique. It would be equally reasonable to compare Kerr and non-Kerr metrics which agree in one or several other observables. For example, one can compare models giving the same accretion efficiency [100], or models giving the same angular offset of the shadow centroid relative to the peak of the accretion disk surface brightness. An exhaustive comparison requires sampling for each Kerr metric the entire parameter space of alternative metrics.

In the following we assume that g gives the black hole metric as a function of the coordinates $x^\mu = t, r, \theta, \phi$. The location of the event horizon of any stationary axially symmetric spacetime can only depend on r and θ . Assuming that the event horizon is a hypersurface defined by a scalar function f and that it is symmetric around the equatorial plane at $\theta = \pi/2$, the null condition $\partial_\mu f \partial^\mu f = 0$ reduces in the equatorial plane to $g^{rr} = g_{rr}^{-1} = 0$ [179, 90]. The event horizon is given by the largest r at which the condition holds.

The properties of circular orbits can be derived from the Lagrangian of a test particle. The presentation of Equations (3)-(13) below follows the concise derivation from Bambi et al. (2017) [17]. See [32, 34, 158] for earlier

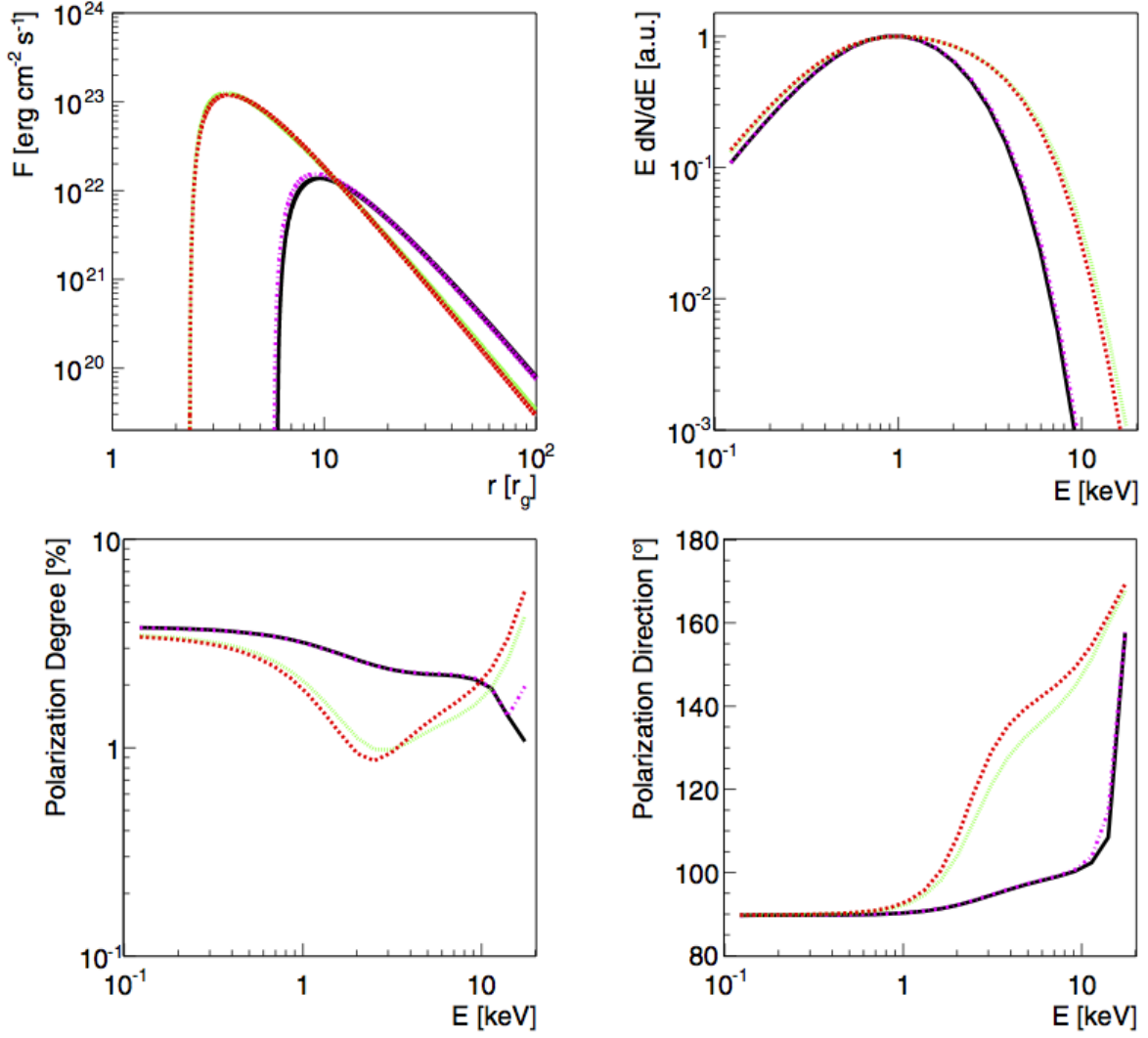


Fig. 4 Accretion disk brightness in the plasma frame (top left), energy spectrum (top right), polarization fraction (bottom left), and polarization angle (bottom right) for two pairs of a Kerr metric and a non-Kerr metric giving similar r_{ISCO} -values. The solid black line and the dashed-dotted magenta lines show the results for the Kerr metric with $a = 0$, $r_{\text{ISCO}} = 6$ and the $m5a$ metric with $a = 0.5$, $\epsilon_3 = -5$, $r_{\text{ISCO}} = 5.8$, respectively. Similarly, the dotted green line and the dashed red line show the results for the Kerr metric with $a = 0.9$ and the $m5a$ metric with $a = 0.5$ and $\epsilon_3 = 6.3$, respectively, both giving $r_{\text{ISCO}} = 2.32$. From [102].

derivations. The Lagrangian is:

$$L = \frac{1}{2} g_{\mu\nu} u^\mu u^\nu \quad (3)$$

with the four velocity $u^\mu = \frac{d}{d\tau} x^\mu$. As L does not depend on t and ϕ , the Euler-Lagrange equations

$$\frac{d}{d\tau} \frac{\partial L}{\partial u^\mu} - \frac{\partial L}{\partial x^\mu} = 0 \quad (4)$$

lead to two constants of motion, the energy and angular momentum per unit mass:

$$-E = g_{tt} u^t + g_{t\phi} u^\phi, \quad L_z = g_{t\phi} u^t + g_{\phi\phi} u^\phi. \quad (5)$$

Denoting the four velocity of equatorial circular orbits with \mathbf{v} , circular orbits require $v^r = \frac{d}{d\tau} v^r = v^\theta = 0$, so that the r -component of the Euler-Lagrange reads:

$$(\partial_r g_{tt})(v^t)^2 + 2(\partial_r g_{t\phi})v^t v^\phi + (\partial_r g_{\phi\phi})(v^\phi)^2 = 0 \quad (6)$$

After dividing by v^ϕ , solving for the orbital frequency $\Omega = v^\phi/v^t$ gives:

$$\Omega = (-\partial_r g_{t\phi} \pm \sqrt{(\partial_r g_{t\phi})^2 - \partial_r g_{tt} \partial_r g_{\phi\phi}}) / \partial_r g_{\phi\phi}. \quad (7)$$

The orbital period of the accreting matter measured by an observer in the asymptotically flat region of the spacetime is given by $P = 2\pi/\Omega$. Figure 6 shows the

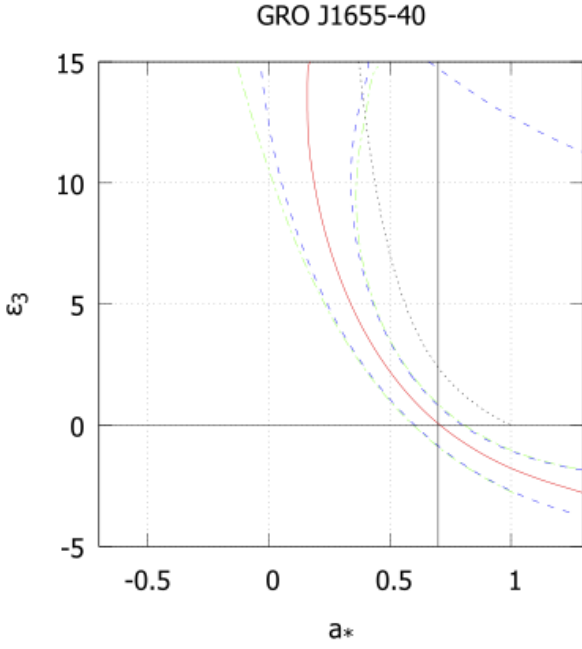


Fig. 5 Constraints on the $m5a$ parameters a and ϵ_3 derived from fitting the energy spectrum of the thermal accretion disk emission predicted for the black hole candidate GRO J1655-40. The red solid curve shows the best fit values. The blue dashed and green dashed-dotted lines show uncertainties resulting from the measurement errors. Reproduced from [100] with permission of the authors.

r -dependence of P for test particles for the Kerr metric, and $m2$ and $m6$ metrics giving the same P at the respective ISCOs.

Writing the four velocity of matter on a circular orbits as:

$$v^\mu = v^t(1, 0, 0, \Omega), \quad (8)$$

v^t follows from the normalization condition $v^2 = 1$:

$$v^t = (-g_{tt} - 2\Omega g_{t\phi} - \Omega^2 g_{\phi\phi})^{-1/2} \quad (9)$$

The constants of motion for equatorial circular orbits follow from the Equations (5):

$$E_{\text{CO}} = -(g_{tt} + \Omega g_{t\phi})v^t, \quad L_{z,\text{CO}} = (g_{t\phi} + \Omega g_{\phi\phi})v^t \quad (10)$$

The ISCO is found by solving for (see e.g. [20], Sect. 12.1):

$$\frac{dE_{\text{CO}}}{dr} = 0. \quad (11)$$

Going back to Equations (5) for arbitrary orbits, the normalization condition $u^2 = 1$ gives:

$$g_{tt}(u^r)^2 + g_{\phi\phi}(u^\theta)^2 + V_{\text{eff}} = 1 \quad (12)$$

with the quasi-potential

$$V_{\text{eff}} = \frac{E^2 g_{\phi\phi} + 2EL_z g_{t\phi} + L_z^2 g_{tt}}{g_{t\phi}^2 - g_{tt}g_{\phi\phi}} \quad (13)$$

From the requirements that $u^r = u^\theta = \frac{d}{d\tau}u^r = \frac{d}{d\tau}u^\theta = 0$ for stable circular orbits, it follows that $V_{\text{eff}} = 1$, and $\partial_r V_{\text{eff}} = \partial_\theta V_{\text{eff}} = 0$ when evaluated in the equatorial plane ($\theta = \pi/2$). Once the ISCO is inferred from Equation (11), one can check the radial and vertical stability conditions for all larger orbits.

One of the pseudo-observables considered below is the redshift of photons coming from certain portions of the accretion disk. For simplicity we assume that the photons are emitted into a direction vertical to the accretion disk as measured by an observer comoving with the emitting plasma with four velocity \mathbf{v}_e . We use a tetrad (an orthogonal set of tangent basis vectors $\mathbf{e}_{(b)}$ normalized to -1, 1, 1, and 1 for the indices $b = 0, 1, 2$, and 3, respectively) defining a Lorentzian coordinate frame for the comoving observer:

$$\mathbf{e}_{(0)} \equiv \mathbf{v}_e, \quad (14)$$

$$\mathbf{e}_{(1)} \equiv g_{rr}^{-1/2} \partial_r, \quad (15)$$

$$\mathbf{e}_{(2)} \equiv g_{\theta\theta}^{-1/2} \partial_\theta, \quad (16)$$

and $\mathbf{e}_{(3)}$ given by the orthonormality conditions. In terms of these basis vectors, the components of the wave vector of photons emitted into the direction $-\partial_\theta$ into the upper hemisphere are $k_e^b = (1, 0, -1, 0)$. The world vector \mathbf{k}_e is thus given by:

$$\mathbf{k}_e = k_e^b \mathbf{e}_{(b)} = \mathbf{e}_{(0)} - \mathbf{e}_{(2)}. \quad (17)$$

which can be used to read off the contravariant components k_e^μ in terms of the coordinate basis vectors $(\partial_t, \partial_r, \partial_\theta, \partial_\phi)$. The time translation symmetry of the considered metrics and the associated Killing vector ∂_t imply that the covariant t -component k_t of the photon's wave vector \mathbf{k} is conserved along the photon geodesic and keeps its value at the time of emission:

$$k_t = (k_e)_t = g_{t\mu} k_e^\mu. \quad (18)$$

The fractional frequency change of the photon between emission in the plasma frame and the detection by a distant receiver at rest in the asymptotically flat region (four velocity $\mathbf{v}_r^\mu = (1, 0, 0, 0)$) is thus given by

$$g_\nu = \frac{\mathbf{v}_r \cdot \mathbf{k}_r}{\mathbf{v}_e \cdot \mathbf{k}_e} = \frac{(k_r)_t}{-1} = -(k_e)_t. \quad (19)$$

The last equality follows from the conservation of k_t along the geodesic.

Page and Thorne (1974) showed that mass, energy, and angular momentum conservation together with the

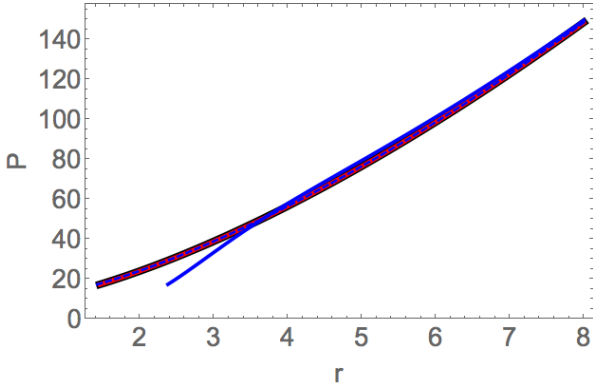


Fig. 6 Orbital periods as a function of the radial coordinate r for the Kerr metric with $a = 0.99$, the $m2$ test metric with $a = 0.872$, $\beta = 0.2254$ and $a = 0.9998$, $\beta = -0.01992$ (all three giving the red solid line), and the $m6$ test metric with $a = 0.05$, $\alpha_{22} = 191.08$ (blue solid line) and $a = 0.999$, $\alpha_{22} = -0.088$ (blue dashed line). A black hole mass of $M = 1$ is assumed and r and P are given in geometric units.

assumption of a vanishing torque at the ISCO determine the radial brightness profile of the accretion disk [138]. The time average flux of radiant energy (energy per unit proper time and unit proper area) flowing out of the upper surface of the disk measured by a co-rotating observer is given by:

$$F(r) = \frac{\dot{M}}{4\pi} e^{-(\nu_0 + \psi + \mu_1)} f(r) \quad (20)$$

with \dot{M} being the mass accretion rate, and ν_0 , ψ , and μ_1 from the metric in standard form (Equation (1)). The function f depends on the four velocity of the orbiting particles and its change with the coordinate r :

$$f(r) = \frac{-v^t_{,r}}{v_\phi} \int_{r_{\text{ISCO}}}^r \frac{v_{\phi,r}}{v^t} dr \quad (21)$$

where “,” denotes ordinary partial differentiation. It is straight forward to solve Equations (20) and (21) numerically. The bolometric luminosity scales with the mass accretion rate \dot{M} and the accretion efficiency η . The latter can be calculated here from the change of a test particle’s energy at infinity as it accretes from infinity to r_{ISCO} : $\eta = 1 - E_{\text{CO}}(r_{\text{ISCO}})$.

The disk emits thermally at a radius-dependent temperature of:

$$T_{\text{eff}}(r) = \left(\frac{F(r)}{\sigma_{\text{SB}}} \right)^{1/4} \quad (22)$$

with σ_{SB} the Stefan Boltzman constant. The emitted energy spectrum can be described by a diluted blackbody spectrum with a hardening factor of f_h . The latter parameter gives the blueshift of the emitted photons owing to the Comptonization of the photons

in the accretion disk atmosphere. For stellar mass black holes, the hardening ratio has a value between 1.5 and 1.7 [168, 42, 43].

In the following we examine a particular Kerr metric with $M = 1$ and $a = 0.99$. Rapidly spinning black holes are the more interesting ones as the accretion disks can extend close to the event horizon, where the strong-gravity effects are most pronounced. The corresponding event horizon is found at $r_{\text{H}} = 1.14$ and the ISCO is located at $r_{\text{ISCO}} = 1.45$. The orbital angular frequency is $\Omega = 0.36$ and the period P is $2\pi/\Omega = 17.24$.

We will compare the Kerr metric with several $m2$ and $m6$ metrics. The metric $m2$ describes black holes rather than naked singularities for (with $M = 1$):

$$a^2 - \beta^2 \leq 1 \quad (23)$$

with an event horizon at:

$$r_+ = 1 + \sqrt{1 - a^2 - \beta^2} \quad (24)$$

The deviation parameter α_{22} of Johannsen’s test metric $m6$ modifies the (t, t) and (t, ϕ) elements of the metric. In the equatorial plane, the event horizon is located at:

$$r_+ = 1 + \sqrt{1 - a^2}, \quad (25)$$

a result formally equal to the one for the Kerr metric. The metric does not exhibit pathologies outside of the event horizon as long as [88]:

$$\alpha_{22} > -(1 + \sqrt{1 - a^2})^2. \quad (26)$$

Unfortunately, Johannsen’s metric yields very unwieldy expressions for most of the quantities of interest ($r_{\text{ISCO}}, \Omega, \dots$) which we do not reproduce here.

Setting $M = 1$, we neglect the fact that M is poorly constrained for many of the systems under study. Possible variations of M exacerbate the problem distinguishing between different metrics. We limit the following discussion to prograde orbits. The same analysis could be performed for retrograde orbits. The condition $P_{\text{ISCO}} = 17.24$ defines one dimensional regions in the $a - \beta$ and $a - \alpha_{22}$ planes. Figure 7 shows these regions as determined by a numerical root finder for valid black hole metrics satisfying Equation (23) or Equation (26). Curves such as the ones shown in Fig. 7 establish maps of the original parameters (a, β) and (a, α_{22}) to the new parameters (P_{ISCO}, a) for the overlapping P_{ISCO} regions. For the Kerr metric P_{ISCO} can take all values between 4π and 52π . The fact that the $m2$ and $m6$ metrics can produce P_{ISCO} -values outside of this range proves criterion *C2* that the two test metrics include

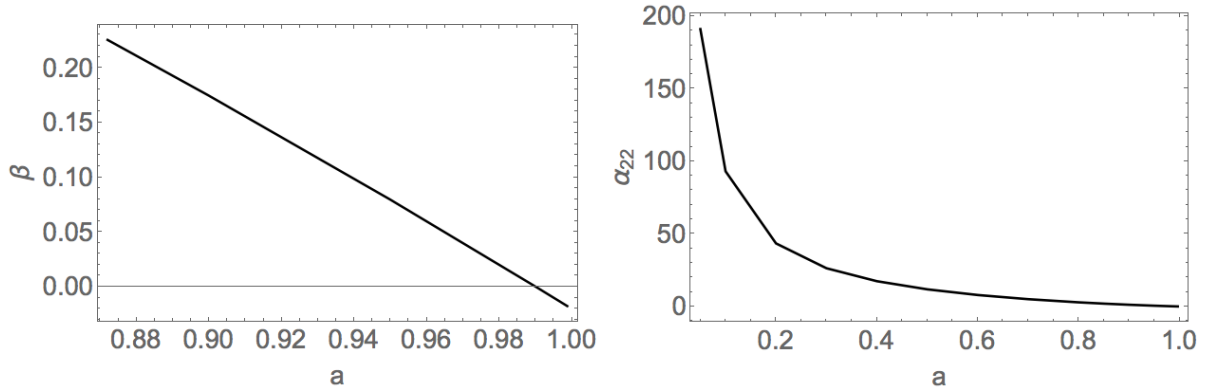


Fig. 7 Combinations of the parameters a and β of the test metric $m2$ (left) and the parameters a and α_{22} of the test metric $m6$ (right) giving the same orbital period at the innermost stable orbit $P_{\text{ISCO}} = 17.24$ as the Kerr metric with $M = 1$ and $a = 0.99$.

spacetimes which are physically distinct from any Kerr spacetime. Note that observational tests in the region of the $m2$ and $m6$ parameter space with $P_{\text{ISCO}} > 52\pi$ face additional problems as disk instabilities might move the inner edge of the disk to r -values r_1 exceeding r_{ISCO} with an associated orbital period $P(r_1) \gg P_{\text{ISCO}}$. The problem can be mitigated somewhat by repeated observations of one and the same object enabling the determination of r_{ISCO} (and/or P_{ISCO}) as the lower bound(s) of the observed values. Criterion $C2$ can further be proven by showing that the different metrics produce non-identical observables for one and the same P_{ISCO} -value. We will do so in the next paragraph.

In the following we will look at a few observables, comparing the Kerr metric with $a = 0.99$, with the nearly-extreme $m2$ metrics with $a = 0.872$, $\beta = 0.2254$ and $a = 0.9998$, $\beta = -0.01992$ and the nearly extreme $m6$ metrics with $a = 0.05$, $\alpha_{22} = 191.08$ and $a = 0.999$, $\alpha_{22} = -0.088$. All metrics give the same $P_{\text{ISCO}} = 17.24$.

Figure 8 shows the fractional frequency change g_ν of vertically emitted photons as a function of the orbital period P . Whereas the two $m2$ metrics and the $m6$ metric with $a = 0.999$ and $\alpha_{22} = -0.088$ give the same g_ν -values, the $m6$ metric with $a = 0.05$ and $\alpha_{22} = 191.08$ gives noticeably smaller g_ν -values (higher redshifts) for $P < 130$ ($r < \sim 7r_g$). The figure indicates that the observations of Fe K α emission from matter spiraling towards the black hole can be used to distinguish between a black hole described by the Kerr metric one of the non-Kerr $m6$ metrics.

Using the equations described above, we can estimate the radial distribution of the temperature T and brightness F of the accretion disk photosphere. Figure 9 shows the product of T and the redshift factor g_ν as a proxy for the energies of the observed photons as a function of P . Interestingly, the results for the Kerr metric,

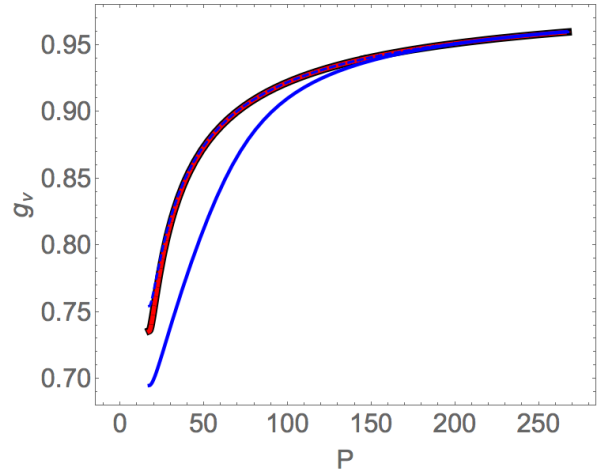


Fig. 8 Net fractional change g_ν of the frequency of vertically (plasma frame) emitted photons reaching an observer at infinity as a function of the orbital period for the Kerr metric with $a = 0.99$ (black solid line, shadowed by the red line), the $m2$ test metric with $a = 0.872$, $\beta = 0.2254$ (red solid line) and $a = 0.9998$, $\beta = -0.01992$ (red dashed line, shadowed by the red line), and the $m6$ test metric with $a = 0.05$, $\alpha_{22} = 191.08$ (blue solid line) and $a = 0.999$, $\alpha_{22} = -0.088$ (blue dashed line).

the two $m2$ metrics, and the $m6$ metric with $a = 0.999$ and $\alpha_{22} = -0.088$ are again indistinguishable. Only the $m6$ metric with $a = 0.05$ and $\alpha_{22} = 191.08$ gives a different distribution with - compared to the distributions for the Kerr metric - lower temperatures closer to the black hole and higher temperatures further away.

Assuming an accretion disk annulus at radius r emits continuum emission at observed energy $E_\gamma \propto g_\nu T$, we can generate pseudo energy spectra by histogramming the temperature of all accretion disk ring annuli with $r \in [r_{\text{ISCO}}, \infty]$ weighing each annulus with the energy flux of the annulus (Figure 10, upper panel).

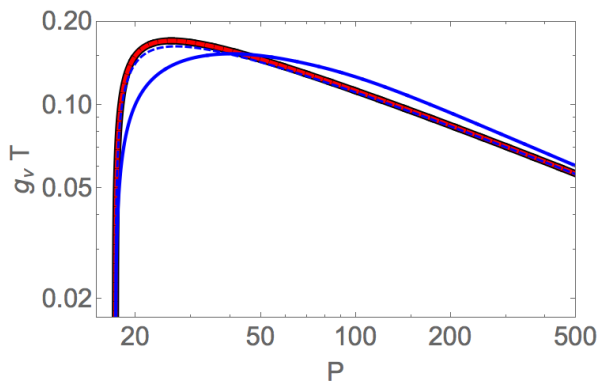


Fig. 9 Product of the photospheric accretion disk temperature times the frequency shift g_ν between emission and observer as a function of the orbital period for the same metrics as in Fig. 8.

As before, only the $m6$ metric with $a = 0.05$ and $\alpha_{22} = 191.08$ gives noticeable deviations. The lower panel of Figure 10 shows that these deviations persist when fine tuning the mass accretion rate \dot{M} and the flux normalization to minimize the difference between the distributions.

To summarize this section: the best strategy for comparing the spacetimes of different metrics is to focus exclusively on observables. Approximate degeneracies between metric parameters can be eliminated by replacing one or more of the degenerate parameters with key observables. Our analysis indicates that the metric $m2$ is not well suited for X-ray tests of the Kerr hypothesis as it barely impacts X-ray observables. In contrast, the metric $m6$ can be used as it does lead to quite different observable outcomes. A full ray-tracing simulation should be used for a more thorough evaluation.

5 Constraining black hole spacetimes with X-ray observations

Two methods for measuring the spins of black holes have been extensively used: (i) fitting the continuum energy spectra of stellar mass black holes in the thermal state, and (ii) modeling the energy spectra from the inner accretion disk, including the Fe $K\alpha$ fluorescent line, and, if observationally accessible, the Compton hump emission. Whereas the first method can only be used for stellar mass black holes in X-ray binaries, the second method can be used for mass accreting stellar mass and supermassive black holes.

The **thermal continuum fitting** method (e.g. [198,69,117]) is based on observing the thermal emission of geometrically thin, optically thick accretion disks. The method requires the independent measure-

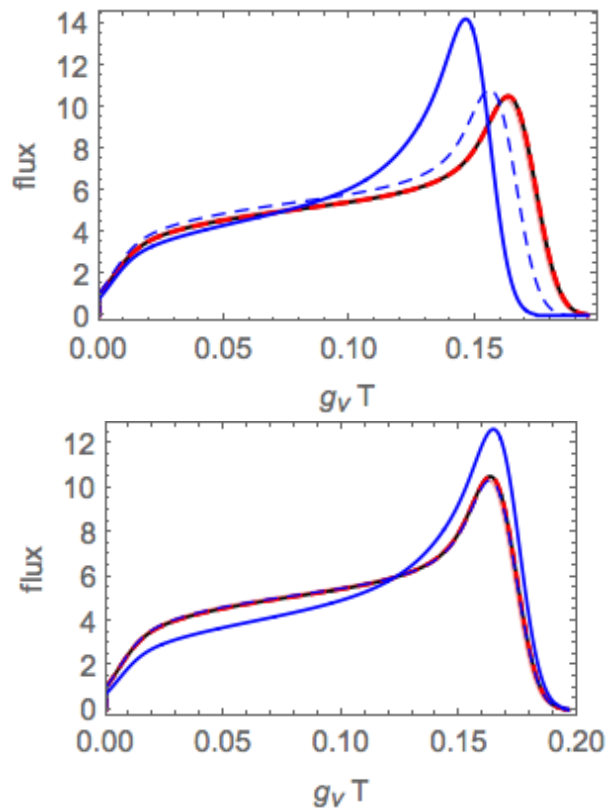


Fig. 10 Distributions of the accretion disk temperatures weighted with the observer frame energy flux for identical accretion rates (top) and after fine tuning the accretion rate and the flux normalization to make the distributions as similar as possible (bottom) for the same metrics as in Fig. 8.

ment of the distance D of the X-ray binary, the black hole mass M , and the inclination i of the binary system. The inclination i is defined as the angle between the angular momentum axis of the binary and the line of sight. These quantities can be inferred from radio, infrared and/or optical observations of the binary system. Assuming that the disk is described by the standard Novikov-Thorne model, and that the angular momentum vectors of the black hole and the binary system are aligned, the X-ray energy spectrum can then be used to fit the black hole spin parameter a (determining the ISCO) and the accretion rate \dot{M} using suitable emission models. State-of-the-art models include relativistic effects (frame dragging, Doppler and gravitational frequency shifts, light bending) and detailed modeling of the emission including limb darkening and spectral hardening, and disk self-irradiation.

The **inner disk reflection modeling** method [51, 29,120,28] relies entirely on modeling the X-ray energy spectra. The reflected emission is thought to originate from the irradiation of the accretion disk photosphere with hard coronal X-ray emission. The gravi-

tational and Doppler frequency shifts broaden the reflected lines, and more so for high spins (small r_{ISCO}) and large inclinations i .

In the following we discuss the results for stellar mass black holes in X-ray binaries as the spins obtained with both methods can be compared to each other. Furthermore, the inclinations inferred from the inner disk reflection modeling can be compared to the non-X-ray constraints on the inclination of the binary orbit. Bambi, Jiang and Steiner (2017) give a compilation of recent continuum fitting and inner disk reflection modeling results. The list includes 19 stellar mass black hole candidates and 25 supermassive black holes [18] (see also [28, 50]).

The spin parameters for all six stellar mass black holes with results from both methods are shown in the left panel of Fig. 11. The confidence intervals are all from the original publications and are usually on the 67% or 90% confidence level for measured values and on the 99% or 3σ confidence level for lower or upper limits. A rough agreement between the results obtained with the two methods can be recognized in the sense that most of the studied black holes have rather high spin parameters exceeding 0.5. For a few of the objects the two methods yield only marginal agreement or even significant disagreement:

Cyg X-1: For Cyg X-1, we have a highly reliable distance estimate of $1.86^{+0.12}_{-0.11}$ kpc from the measurement of a trigonometric parallax with the Very Long Baseline Array [148] and good constraints on the mass of the companion $M_* = (19.2 \pm 1.9)M_\odot$, the mass of the black hole $M_{\text{BH}} = (14.8 \pm 1.0)M_\odot$, and the inclination of the binary orbit $i = 27.1^\circ \pm 0.8^\circ$ [137]. The spin parameter result $a > 0.983$ (3σ) from the thermal continuum method [75] is thus particularly well supported by observations. The inner disk reflection modeling gives a wide range of different results: $0.6 \leq a \leq 0.99$ [121], $a = 0.838 \pm 0.006$ [182], $a = 0.88^{+0.07}_{-0.11}$ [47], $0.93 \leq a \leq 0.96$ [189], $a = 0.949^{+0.013}_{-0.019}$ [183], $a = 0.97^{+0.014}_{-0.02}$ [53], $a = 0.9882^{+0.009}_{-0.009}$ [182], and $a > 0.987$ [183].

GRO 1655–40: Whereas the thermal continuum fitting method gives $0.55 \leq a \leq 0.85$ [167], the inner disk reflection modeling gives $a > 0.9$ [150]. The discrepancy seems to be significant as both groups go through a number of models with all thermal continuum fitting results < 0.85 and all inner disk reflection modeling results > 0.9 .

GRS 1915+105: McClintock et al. (2006) present a thermal continuum fitting analysis indicating $a > 0.98$ [118]. The authors give a very detailed evaluation of the impact of various observational uncertainties on the results, showing that substantially

lower spin parameters ($a \sim 0.8$) are less likely but possible. Middleton et al. (2006) get a significantly lower thermal continuum result of $a = 0.72^{+0.009}_{-0.017}$ [119], a discrepancy which might result from using intermediate rather than low luminosity observations for the analysis [118]. Reid et al. (2014) derive another continuum fitting result of $a > 0.92$. Miller et al.’s (2013) inner disk reflection modeling indicates a near-extremal spin parameter of $a = 0.98^{+0.01}_{-0.01}$ [122].

GX 339–4: Kolehmainen & Done (2011) set a limit of $a < 0.9$ on the spin parameter of GX 339–4 from the analysis of the thermal continuum emission [99] which is lower than the inner disk reflection modeling results of $a = 0.935 \pm 0.01$ (statistical) ± 0.01 (systematic) by Reis et al. [151], $a = 0.95^{+0.03}_{-0.05}$ by García et al. [66], and $a = 0.95^{+0.02}_{-0.08}$ by Parker et al. [142].

The discussion shows the systematic errors are still large ($\Delta a \sim 0.1 - 0.2$), as evident from the different results obtained with one and the same method (Cyg X-1 and GRS 1905+105), and with the two complementary methods (GRO 1655–40 and GX 339–4).

Similarly interesting is the comparison of the orbital inclination and the inclination of the inner disk from the inner disk reflection modeling. The right panel of Fig. 11 shows consistent results for GRS 1915+105, SWIFT J1753.5-0127, V404 Cygni, XTE J1550-564, XTE J1650-500, and MAXI J1836-194. For Cyg X-1, GRO 1655–40, and GX 339–4 there are significant deviations:

Cyg X-1: The modeling of the optical photometric and spectroscopic data indicates a near face-on inclination of $i = 27.1^\circ \pm 0.8^\circ$ [137]. The inner disk reflection modeling gives a wide range of inclinations $i < 20^\circ$ [183], $i = 23.7^\circ - 5.4^\circ + 6.7^\circ$ [53], $i = 32^\circ \pm 2^\circ$ [47], $i = 37.5^\circ \pm 0.7^\circ$ [183], $37.6^\circ \leq i \leq 41.3^\circ$ [189], $i = 53.9^\circ \pm 0.4^\circ$ and $i = 69.2^\circ - 0.9^\circ + 0.5^\circ$ [182].

GRO 1655–40: The inclination $i = 70.2^\circ \pm 1.9^\circ$ [76] deviates significantly from the inner disk reflection modeling result of $i = 30^\circ - 5^\circ + 10^\circ$ [150].

GX 339–4: Kolehmainen & Done (2010) argue for a likely orbital inclination of between 50° and 70° [98]. The inner disk reflection modeling gives a range of results: $i < 20^\circ$ [151], $i = 40^\circ - 60^\circ$ [61], $i = 30^\circ \pm 1^\circ$ [142], and $i = 48^\circ \pm 1^\circ$ [66].

The discrepancies could result from a misalignment of the inner disk and the binary orbit (see [111, 115]). If the angular momentum vectors of the black hole and the binary system are not aligned a Bardeen-Petterson

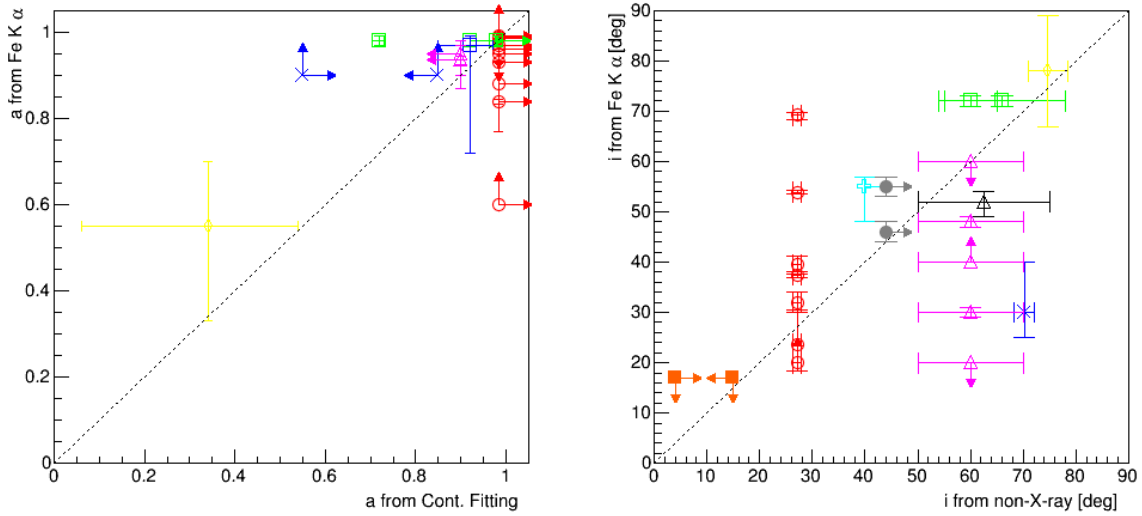


Fig. 11 The left panel compares the black hole spin parameter estimates from the continuum fitting method and the inner reflection modeling for the stellar mass black holes Cyg X-1 (red open circles) [75, 47, 53, 121, 182, 189, 183], GRO 1655-40 (blue crosses) [167, 150], GRS 1915+105 (open green squares) [118, 119, 122, 149], GX 339-4 (open magenta triangles) [98, 151, 66, 142], LMC X-1 (blue open squares) [73, 173], XTE J1550-564 (yellow diamond) [174, 171]. The right panel compares the inclinations from non-X-ray observations and inner reflection modeling for the black holes Cyg X-1 (red open circles) [137, 53, 47, 189, 182, 183], GRO 1655-40 (blue cross) [76, 150], GRS 1915+105 (open green squares) [54, 122, 149], GX 339-4 (open magenta triangles) [98, 151, 61, 66, 142], MAXI J1836-194 (filled orange squares) [157, 152], SWIFT J1753.5-0127 (open cyan cross) [131, 150], V404 Cygni (black open triangle) [95, 190], XTE J1550-564 (yellow diamond) [174, 173], and XTE J1650-500 (grey filled circles) [136, 123, 188].

type configuration may result with the inner accretion disk orbiting the black hole in its equatorial plane and the outer disk being aligned with the binary orbit (see the discussion in Sect. 6).

How would the thermal continuum black hole spin parameters change if one would use the inclinations from the inner disk reflection modeling in the analysis? For Cyg X-1 the thermal continuum fitting spin parameter would drop from close to 1 to $a \sim 0.96$ when changing the inclination from $i \approx 20^\circ$ to $i \approx 40^\circ$ ([74], Fig. 5) making it consistent with the spin parameter ($0.93 \leq a \leq 0.96$) and inclination ($37.6^\circ \leq i \leq 41.3^\circ$) results of Walton et al. (2016) [189]. The high inclination of $i = 69.2^\circ$ from the inner disk reflection model #4 of Tomsick et al. (2014) would bring the thermal continuum fitting spin parameter down to $a \sim 0.9$, significantly lower than the corresponding inner disk reflection spin parameter of $a = 0.9882_{-0.009}^{+0.009}$. Using the inclination of $i = 53.9^\circ$ from the inner disk reflection model #8 of Tomsick's paper would bring the thermal continuum fitting spin parameter down to $a \sim 0.93$, still significantly higher than the spin parameter of $a = 0.838 \pm 0.006$ from the inner disk reflection modeling. For GRO 1655-40, using the inclination $i \approx 30^\circ$ from the inner disk reflection modeling instead of the orbital inclination of $i \approx 70^\circ$ would resolve the discrepancy be-

tween the thermal continuum fitting results ($a < 0.85$) and the inner disk reflection modeling ($a > 0.9$). The misalignment hypothesis can thus resolve some but not all of the discrepancies. Note that Steiner et al. constrain the jet-disk misalignment to be less than 12° for one particular source (XTE J1550-564) [171].

If we adopt the hypothesis that the inner accretion disks of some stellar mass black holes are misaligned, the main concern evident from Fig. 11 are the widely different results obtained with one and the same method for the well studied objects Cyg X-1 and GRS 1915+105. McClintock et al. (2006) explain the difference between their and Middleton et al.'s thermal continuum fitting results by the use of different data sets. They argue that the observations of low-luminosity ($L_X < 0.3L_{\text{Edd}}$) rather than intermediate-luminosity thermal state observations give the most reliable results. At higher luminosities the disk may acquire a non-negligible thickness, and the relative importance of a non-vanishing torque at r_{ISCO} may increase. Analyzing a large number of low-luminosity data sets, McClintock et al. (2006, 2014) [118, 117] find excellent agreement for all the individual results. Noble et al. (2011) [134], Kulkarni et al. (2011) [105], and Zhu et al. (2012) [200] study the impact of a non-vanishing inner torque on the radial emission profile and the inferred

thermal continuum fitting spin parameter results based on GRMHD simulations. They find that the associated systematic errors are rather small, especially for high spins (e.g. $\Delta a \sim 0.3, 0.1, 0.03, 0.01$ for spin parameters of $a < 0.5, a = 0.7, 0.9$, and 0.98 , respectively). One major theoretical uncertainty of the thermal continuum fitting method is the spectral hardening by a factor $\sim f_h$ impacting the mean energy of thermally emitted photons $E_\gamma \approx 2.70 f_h k_B T$ where k_B is the Boltzmann constant. For example, Shafer et al. (2006) [167] find that the thermal continuum spin parameters of the two black holes GRO J1655-40 and 4U 1543-47 ($a \sim 0.7$) change by about $\Delta a \approx 0.1$ between the spectral hardening models of Shimura & Takahara (1995) [168] and Davis et al. (2005) [42].

The **inner disk reflection modeling** depends on disentangling the continuum emission, the reflection component, and absorption features (see e.g. [99, 28]). A broad bandpass as that afforded by NASA's *NuSTAR* mission helps to do so (e.g. [155]). The fit models depend on assumptions about the geometry and physical properties of the accretion disk, the accretion disk photosphere, and the corona (or the emissivity profile). Usually, the accretion disk is assumed to extend from r_{ISCO} to infinity and the corona is assumed to be a point source of (in its rest frame) isotropic emission hovering above the black hole. Alternatively, a certain functional form of the emission profile (i.e. the radial dependence of the coronal flux impinging on the accretion disk, prompting the emission of Fe K α photons) is assumed (e.g. a single power law or a broken power law) and the analysis includes fitting a number of parameters describing the emissivity profile. The line shapes and equivalent widths are assumed to depend only on the metallicity of the plasma, and the ionization parameter. These assumptions may not be correct:

- The material in the plunging region between the event horizon and the inner edge of the accretion disk may modify the observed line shapes (however, see the discussions in [120]).
- Accretion disks may have an inner cutoff at $r_1 > r_{\text{ISCO}}$, they may have non-negligible thicknesses, and they may be warped or clumpy.
- The ionization degree and density of the photospheric plasma may vary strongly as a function of the radial coordinate [65].
- The coronas may have different and/or time varying geometries, see [41, 63, 72].
- The emission from some parts of the accretion disks may be absorbed.

Various authors noted that some of the observed Fe K α lines requires unrealistically high metallicities exceeding solar metallicities by factors as large as ten

or higher, indicating that the inner reflection line modeling is still missing important physics (see [154, 63] and references therein). García et al. 2016 show that the density of the photospheric plasma strongly impact the shapes of the reflected lines [65]. Tomsick et al. (2018) fit *NuSTAR* and *Suzaku* observations of Cyg X-1 and find that a higher-density model gives substantially different metallicity, spin, and inclination results [183].

Figure 11 and the systematic errors and uncertainties described above indicate that the X-ray constraints on black hole spin parameters and inclinations as well as X-ray tests of the Kerr hypothesis have to be received with some caution. We will discuss possible avenues for further progress in the next section.

6 Discussion

According to the Kerr hypothesis, astrophysical quasi-stationary black holes are macroscopic elementary particles can be described by four continuous parameters (mass, angular momentum magnitude, and angular momentum orientation). As quasi-stationary black holes play important roles in galaxies and galaxy clusters, and describe key objects involved in gravitational wave events, it is highly desirable to test this prediction as accurately as possible. X-ray tests are independent and complementary to tests based on gravitational waves, radio interferometric observations of black hole shadows, and the observations of stars orbiting supermassive black holes. The discussion above can be summarized as follows:

1. The Kerr family of metrics describes a wide range of physically different spacetimes. Many of the proposed alternative metrics produce very similar spacetimes.
2. Solar system and binary tests of GR are based on observations of isolated test bodies in stable orbits, enabling precision measurement of the properties of the underlying spacetime. In the case of X-ray observations of black holes, we see the emission from accretion disks: viscous, self-interacting, non-linear, macroscopic objects. Small differences of the underlying spacetime are easily drowned by the averaging over different orbits effected by the turbulence of the accreting plasma. The macroscopic properties of the disk are then largely determined by energy, mass, and angular momentum conservation.
3. Although the numerical modeling of black hole accretion has made enormous progress over the last two decades, the observational outcomes depend on the proper modeling of many different physical processes. The observational outcomes may depend on

the detailed properties of the magnetized, partially ionized plasma, and the detailed phase space distributions of photons and electrons. We may still be far away from a sufficiently complete understanding of which properties and processes play an important role and which ones may be neglected.

4. Even if the numerical simulations captured all the relevant physical processes, the problem of mapping the observations to a certain accretion flow configurations may be ill defined. It may simply not be possible to use the observations to constrain all the relevant properties of the accretion flow (e.g. the shape and location of the corona, the alignment of the black hole spin and the angular momentum vector of the accretion disk, and the properties of the accreted magnetic field) sufficiently well to allow for quantitative tests of the Kerr hypothesis.
5. The analysis of the X-ray observations are plagued by several practical challenges contributing uncertainties to the derived results, including the selection of suitable data sets and the accurate modeling of the contributions from other emission components.

The spin parameter and inclination results discussed in Sect. 5 indicate that the current uncertainties are rather large. For example, the spin parameter seems to be uncertain by $\Delta a \sim 0.1 - 0.2$. The finding emphasizes the difficulties one faces when using the X-ray data for quantitative tests of GR.

Several upcoming missions and missions in development can add new information about the inner accretion flows:

X-ray polarimetry: The *Imaging X-ray Polarimetry Explorer (IXPE)* [191], NASA's first dedicated X-ray polarimetry mission is scheduled for launch in 2021 and will measure the polarization of X-ray sources in the 2-8 keV energy band. The mission will acquire high signal-to-noise observations of bright stellar mass black holes in X-ray binaries and first polarimetric results for a number of nearby Seyfert 1 galaxies. The polarization of the thermal continuum emission of mass accreting stellar mass black holes will give new constraints on the orientation of the angular momentum vector of the inner accretion disk and improved measurements of the black hole spin parameter [108, 162, 102]. *IXPE* and balloon borne experiments like *X-Calibur* [96] will test hypotheses about the physical properties of the corona of accreting stellar mass and supermassive black holes [163, 164, 104, 21] and the nature of the reflected emission [45, 113]. We expect that X-ray polarization observations will allow us to validate (or falsify) the current accretion disk and corona models in a similar way as broadband X-ray observations of stellar mass and su-

permassive black holes with *NuSTAR* have tested the reflection nature of the Fe K α line emission (e.g. [155]).

High-throughput X-ray spectroscopy: Future high-throughput X-ray spectroscopy missions such as the upcoming Advanced Telescope for High-ENergy Astrophysics (*ATHENA*) mission of the European Space Agency (anticipated launch: 2028) [129], the Spectroscopic Time-Resolving Observatory for Broadband Energy X-rays (*STROBE-X*) [195], or the Enhanced Timing and X-ray Polarimetry mission (*eXTP*) of the Chinese Academy of Sciences [199] can perform time resolved studies of the Fe K α emission. As mentioned above, sensitive observations of frequency shifts (owing to gravitational and Doppler frequency shifts) as a function of the distance from the black hole (encoded in the orbital modulations of the signal) might be able to distinguish between Kerr and non-Kerr spacetimes (see also [26]).

Black Hole Imager: Ultimately, we would like to image accretion disks. Currently, the Event Horizon Telescope (EHT) combines the 230 GHz data from several Very Long Baseline Interferometry (VLBI) telescopes around the Earth. The expected angular resolution of between 15 and 20 μ arcsec of the EHT is comparable to the angular extents of the supermassive black holes at the centers of Sgr A* and M 87 (e.g. [11]). The first results are expected to be announced soon. Similar angular resolutions might be obtained in the X-ray regime in the more distant future using interferometric techniques or transmissive, refractive-diffractive optics [23]. The radio and X-ray observations would be impacted by very different astrophysical and instrumental systematics. Obtaining images with both techniques would thus be highly desirable.

Continued observations with *Chandra*, *XMM-Newton*, *NICER*, and *NuSTAR* as well as observations with future experiments are likely to open up new ways of testing the Kerr hypothesis:

Observations of microlensed quasars: The X-ray observations of some gravitationally lensed quasars show evidence for microlensing by stars. The amplitude distribution of the flux variations indicate that the X-ray bright regions (i.e. the X-ray emitting coronas) of the microlensed quasars are smaller than $\sim 30 r_g$ [37, 40, 127, 128, 24, 112]. For some of the lensed sources, the energy spectra show evidence for the relativistically broadened Fe K α emission [36, 153, 38]. The *Chandra* observations of the lensed quasars RX J1131-1231, SDSS 1004+4112, QJ 0158-4325, and MG J0414+0534 reveal a shift of the line centroid for some of the obser-

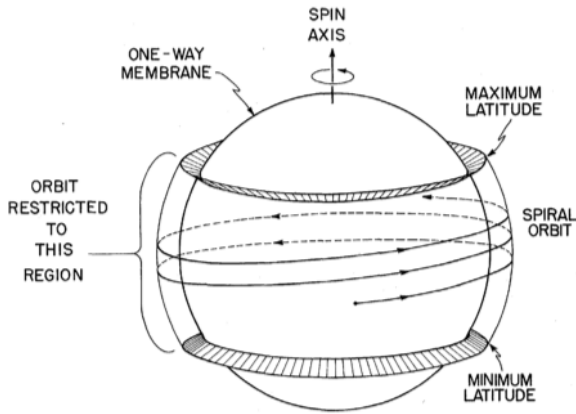


Fig. 12 Part of an inclined test particle orbit around a maximally rotating Kerr black hole showing a corkscrew pattern close to the event horizon rather than the nodal advance for Lense-Thirring precession of orbits further away from the black hole (from [194]).

vations, and multiple lines for others [36, 38, 35]. A possible explanation for the observations is that the line shifts are caused by the selective amplification of the emission from certain regions of the accretion disk as the microlensing caustics move across the system [35, 38, 103]. Based on this paradigm, Chartas et al. (2017) use the energies of the detected lines to constrain the inclination and spin parameter of RX J1131–1231. The observations offer a variant on the inner disk reflection modeling, and share many of the same systematics. In particular, the analysis of the observational data relies on the modeling of the Fe K α emission. The amplification of the X-rays from different regions of the accretion disk and the corona do add new information about the inner accretion flow. However, the results also depend on a number of additional parameters, i.e. the convergence and shear of the macrolens and the location, orientation, and scale of the microlensing caustic(s). Acquiring observations over many years from many different caustic crossings, as well as dense observational sampling of a single caustic crossing might make it possible to overconstrain the quasar and lens parameters.

Observations of Relativistic Precession: The thin disk theory described above applies for systems with parallel black hole and accretion disk angular momentum vectors. Misaligned systems can show much richer dynamics owing to the interplay of relativistic frame dragging and the turbulence of the accreting plasma. The effect of frame dragging on test particles orbiting a spinning body of mass M and angular momentum a is commonly referred to as Lense-Thirring precession of the orbits. Far away from the spinning body, the frame dragging advances the nodes of circular orbits by an angle $\Delta\Omega = 2(a/M)(M/r)^{3/2}$ per revolution

[107]. Close to a black hole, the frame dragging effects are so strong that test particles orbit on corkscrew-type trajectories (Fig. 12) [194]. The combination of the precessing orbits and the turbulence may produce a Bardeen-Petterson-type configuration with the inner disk orbiting the black hole in the equatorial plane of the black hole out to a characteristic radius beyond which the disk maintains its original misalignment [19, 141, 106, 201]. Alternatively, warps may propagate with the speed of sound giving rise to bending waves with a periodically changing disk inclination at a given distance from the black hole [140, 44, 84, 110]. The relativistic precession of the inner disk may cause the low-frequency quasi-periodic oscillations (LFQPOs, 0.1–30 Hz) of the X-ray fluxes from accreting neutron star and black hole sources (e.g. [175, 176, 161, 80, 185, 170]). Ingram and Done (2009) [80] speculate that the inner disk precesses like a solid object. Based on this paradigm, Ingram et al. (2015, 2017) [81, 82] explain the quasi-periodic variations of the energy of the reflected Fe K α line in GRS 1915+105 and H 1743–322 as the result of the reflection of the coronal emission off a precessing inner accretion disk. The net precession depends on the underlying spacetime through the range of available stable orbits and the properties of these orbits. The confrontation of semi-analytical models of misaligned accretion systems with the results from GRMHD simulation (see [59, 60, 202, 125]) will lead to a better understanding of the relevant physical processes. X-ray polarimetry will give us new observational constraints on the orientation of the inner accretion disks and can be used for sensitive searches for such precession effects [81].

Observations of Quasi-Periodic Oscillations (QPOs): The light curves of several black holes in low-mass X-ray binaries (LMXBs) exhibit QPOs identified as peaks in the power density spectra (PDS) [147, 186, 197]. If high-frequency quasi-periodic oscillations (HFQPOs, 40–450 Hz) were directly related to the frequencies of test particle orbits (i.e. the orbital frequency, the radial and vertical epicyclic frequencies, and the Lense-Thirring precession frequency), QPOs could be powerful tools for constraining the underlying spacetime (e.g. [10, 8]). It seems more likely however, that the QPO frequencies result from a complex interplay of the orbital kinematics and the highly non-linear properties of the accretion disk plasma, making the observed frequencies and implications for the underlying spacetime highly model dependent. Intriguingly, QPOs are only found in hard state light curves, not in the thermal state light curves. The finding indicates that the geometrically thin and optically

thick accretion disks responsible for the thermal state emission reach down to the ISCO and do not precess.

Confronting the observational results from ongoing and upcoming X-ray missions with higher fidelity numerical models promises to give us new insights into the physics of black hole accretion, and should eventually give us more reliable constraints on the properties of the underlying background spacetimes.

Acknowledgements I thank Q. Abarr, B. Beheshtipour, P. Bolt, M. Errando, C. Gammie, J. García, B. Groebe, A. Ingram, F. Kislak, and J. Miller for highly enjoyable and helpful discussions. I am grateful to the anonymous referees whose excellent comments improved the paper substantially. I acknowledge NASA funding through the awards 80NSSC18K0264 and NNX16AC42G.

References

1. Abbott, B. P., et al. (LIGO Scientific Collaboration), “Observation of Gravitational Waves from a Binary Black Hole Merger”, *Phys. Rev. Lett.* 116, 061102 (2016).
2. Abbott, B. P., et al. (LIGO Scientific Collaboration), “Tests of General Relativity with GW150914”, *Phys. Rev. Lett.* 116, 1101 (2016).
3. Abbott, B. P., et al. (LIGO Scientific Collaboration), “GW151226: Observation of Gravitational Waves from a 22-Solar-Mass Binary Black Hole Coalescence”, *Phys. Rev. Lett.* 116, 241103 (2016).
4. Abbott, B. P., et al. (LIGO Scientific Collaboration), “GW170104: Observation of a 50-Solar-Mass Binary Black Hole Coalescence at Redshift 0.2”, *Phys. Rev. Lett.* 118, 221101 (2017).
5. Abbott, B. P., et al. (LIGO Scientific Collaboration), “GW170608: Observation of a 19-solar-mass Binary Black Hole Coalescence”, *ApJ*, 851L, 35 (2017).
6. Abbott, B. P., et al. (LIGO Scientific Collaboration), “GW170814: A Three-Detector Observation of Gravitational Waves from a Binary Black Hole Coalescence”, *Phys. Rev. Lett.* 119, 141101 (2017).
7. Abbott, B. P., et al. (LIGO Scientific Collaboration), “GW170817: Observation of Gravitational Waves from a Binary Neutron Star Inspiral”, *Phys. Rev. Lett.* 119, 161101 (2017).
8. Abramowicz, M. A., “QPO as the Rosetta Stone for understanding black hole accretion”, *AN*, 326, 782A (2005).
9. Abramowicz, M. A., Fragile, P. C., “Foundations of Black Hole Accretion Disk Theory”, *Living Rev. Relativ.* 16:1 (2013) [<https://doi.org/10.12942/lrr-2013-1>].
10. Abramowicz, M. A., Kluźniak, W., “A precise determination of black hole spin in GRO J1655-40”, *A&A*, 374L, 19A (2001).
11. Akiyama, K. Kuramochi, K., Ikeda, S., et al., “Imaging the Schwarzschild-radius-scale Structure of M87 with the Event Horizon Telescope Using Sparse Modeling”, *ApJ*, 838, 1 (2017), and [<http://eventhorizontelescope.org>].
12. Aliev, A. N., Gümrükçüoğlu, A. E., “Charged rotating black holes on a 3-brane”, *Phys. Rev. D*, 71j4027A (2005).
13. Ayzenberg, D., Yunes, N., “Black hole continuum spectra as a test of general relativity: quadratic gravity”, *CQGr*, 34k5003A (2017).
14. Balbus, S. A., Hawley, J. F., “Instability, turbulence, and enhanced transport in accretion disks”, *Reviews of Modern Physics*, 70, 1 (1998).
15. Bambi, C., “A Code to Compute the Emission of Thin Accretion Disks in Non-Kerr Spacetimes and Test the Nature of Black Hole Candidates”, *ApJ*, 761, 174B (2012).
16. Bambi, C., “Testing the space-time geometry around black hole candidates with the analysis of the broad $K\alpha$ iron line”, *Phys. Rev. D*, 87b3007B (2013).
17. Bambi, C., Cárdenas-Avendaño, A., Dauser, T., García, J. A., Nampalliwar, S. “TESTING THE KERR BLACK HOLE HYPOTHESIS USING X-RAY REFLECTION SPECTROSCOPY”, *ApJ*, 842, 76B (2017).
18. Bambi, C., Jiang, J., Steiner, J. F., “Testing the no-hair theorem with the continuum-fitting and the iron line methods: a short review”, *Class. Quantum Grav.*, 33, 064001 (2016).
19. Bardeen, J. M., Petterson, J. A., “THE LENSE-THIRRING EFFECT AND ACCRETION DISKS AROUND KERR BLACK HOLES”, *ApJ*, 195, L65-L67 (1975).
20. Baumgarte, T. W., Shapiro, S. L., “Numerical Relativity: Solving Einstein’s Equations on the Computer” Publisher: Cambridge University Press; 1 edition (2010).
21. Beheshtipour, B., Krawczynski, H., Malzac, J., “The X-Ray Polarization of the Accretion Disk Coronae of Active Galactic Nuclei”, *ApJ*, 850, 14B (2017).
22. Berti, E., et al., “Testing general relativity with present and future astrophysical observations”, *Class. Quantum Grav.*, 32, 243001 (2015).
23. The Black Hole Imager [<https://bhi.gsfc.nasa.gov>].
24. Blackburne, J. A., Kochanek, C. S., Chen, B., Dai, X., Chartas, G., “The Structure of HE 1104-1805 from Infrared to X-Ray”, *ApJ*, 798, 95B (2015).
25. Blandford, R. D., Znajek, R. L., “Electromagnetic extraction of energy from Kerr black holes”, *MNRAS*, 179, 433 (1977).
26. Boller, T., Müller, A., “Observational Tests of the Pseudo-complex Theory of GR Using Black Hole Candidates”, In: Greiner W. (eds) *Nuclear Physics: Present and Future*. FIAS Interdisciplinary Science Series. Springer, Cham, pp 245-253 (2015).
27. Boyer, R. H., Lindquist, R. W., “Maximal Analytic Extension of the Kerr Metric”, *J. Math. Phys.*, 8, 265 (1967).
28. Brenneman, L., “Measuring Supermassive Black Hole Spins in AGN”, *Acta Polytechnica Suppl.*, 53, 652 (2013).
29. Brenneman, L. W., Reynolds, C. S., “Constraining Black Hole Spin via X-Ray Spectroscopy”, *ApJ*, 652, 1028B (2006).
30. Cardoso, V., Pani, P., Rico, J., “On generic parametrizations of spinning black-hole geometries”, *Phys. Rev. D*, 89, 064007 (2014).
31. Carroll, S., “Spacetime And Geometry: An Introduction To General Relativity”, Pearson, first edition, Appendix B (2003).
32. Carter, B., “Global Structure of the Kerr Family of Gravitational Fields”, *Phys. Rev.*, 174, 1559 (1968).
33. Castor, J. I., “Radiation Hydrodynamics”, Cambridge University Press (2004).
34. Chandrasekhar, S., “The Mathematical Theory of Black Holes”, Oxford University Press, New York (1983, Reprint 2010).
35. Chartas, G., Agol, E., Eracleous, M., Garmire, G., Bautz, M. W., Morgan, N. D., “Caught in the Act: Chandra Observations of Microlensing of the Radio-loud Quasar MG J0414+0534”, *ApJ*, 568, 509C (2002).

36. Chartas, G., Kochanek, C. S., Dai, X., Moore, D., Mosquera, A. M., Blackburne, J. A., "Revealing the Structure of an Accretion Disk through Energy-dependent X-Ray Microlensing", *ApJ*, 757, 137C (2012).
37. Chartas, G., Kochanek, C. S., Dai, X., Poindexter, S., Garmire, G., "X-Ray Microlensing in RXJ1131-1231 and HE1104-1805", *ApJ*, 693, 174 (2009).
38. Chartas, G., Krawczynski, H., Zalesky, L., Kochanek, C. S., Dai, X., Morgan, C. W., Mosquera, A., "Measuring the Innermost Stable Circular Orbits of Supermassive Black Holes", *ApJ*, 837, 26C (2017).
39. Chiang, C.-Y., Walton, D. J., Fabian, A. C., Wilkins, D. R., Gallo, L. C., "Modelling the extreme X-ray spectrum of IRAS 13224-3809", *MNRAS*, 446, 759 (2015).
40. Dai, X., Kochanek, C. S., Chartas, G., Kozłowski, S., Morgan, C. W., Garmire, G., Agol, E., "The Sizes of the X-ray and Optical Emission Regions of RXJ 1131-1231", *ApJ*, 709, 278D (2010).
41. Dauser, T., Garcia, J., Wilms, J., "Irradiation of an accretion disc by a jet: general properties and implications for spin measurements of black holes", *MNRAS*, 430, 1694-1708 (2013).
42. Davis, S. W., Blaes, O. M., Hubeny, I., Turner, N. J., "Relativistic Accretion Disk Models of High-State Black Hole X-Ray Binary Spectra", *ApJ*, 621, 372D (2005).
43. Davis, S. W., Done, C., Blaes, O. M., "Testing Accretion Disk Theory in Black Hole X-Ray Binaries", *ApJ*, 647, 525 (2006).
44. Demianski, M., Ivanov, P. B., "The dynamics of twisted accretion disc around a Kerr black hole", *A&A*, 324, 829D (1997).
45. Dovčiak, M., Karas, V., Matt, G., et al., "Polarization signatures of strong gravity in active galactic nuclei accretion discs", *MNRAS*, 355, 1005D (2004).
46. Dovčiak, M. & Done, C., "Minimum X-ray source size of the on-axis corona in AGN", *AN*, 337, 441 (2016).
47. Duro, R., Dauser, T., Wilms, J., "The broad iron K α line of Cygnus X-1 as seen by *XMM-Newton* in the EPIC-pn modified timing mode", *A&A*, 533, L3 (2011).
48. Edelson, R., Gelbord, J. M., Horne, K., et al., "Space Telescope and Optical Reverberation Mapping Project. II. Swift and HST Reverberation Mapping of the Accretion Disk of NGC 5548", *ApJ*, 806, 129 (2015).
49. Elvis, M., Wilkes, B. J., McDowell, J. C., et al., "Atlas of quasar energy distributions", *ApJS*, 95, 1 (1994).
50. Fabian, A. C., "The innermost extremes of black hole accretion", *AN*, 337, 375F (2016).
51. Fabian, A. C., Rees, M. J., Stella, L., White, N. E., "X-ray fluorescence from the inner disc in Cygnus X-1", *MNRAS*, 238, 729F (1989).
52. Fabian, A. C., Zoghbi, A., Ross, R. R., et al., "Broad line emission from iron K- and L-shell transitions in the active galaxy 1H0707-495", *Nature*, 459, 540 (2009).
53. Fabian, A. C., Wilkins, D. R., Miller, J. M., "On the determination of the spin of the black hole in Cyg X-1 from X-ray reflection spectra", *MNRAS*, 424, 217 (2012).
54. Fender, R. P., Garrington, S. T., McKay, D. J., et al., "MERLIN observations of relativistic ejections from GRS 1915+105", *MNRAS*, 304, 865F (1999).
55. Feng, Y., Ramesh, N., "Hot Accretion Flows Around Black Holes", *ARA&A*, 52, 529 (2014).
56. Fock, V., "The Theory of Space, Time and Gravitation", Pergamon Press, New York, (1964).
57. Fodor, G., "Multipole moments of axisymmetric systems in relativity", *Journal of Mathematical Physics*, 30, 2252 (1989).
58. Foucart, F., Chandra, M., Gammie, C. F., Quataert, E., Tchekhovskoy, A., "How important is non-ideal physics in simulations of sub-Eddington accretion on to spinning black holes?", *MNRAS*, 470, 2240F (2017).
59. Fragile, P. C., Blaes, O. M., Anninos, P., Salmonson, J. D., "GLOBAL GENERAL RELATIVISTIC MAGNETOHYDRODYNAMIC SIMULATION OF A TILTED BLACK HOLE ACCRETION DISK", *ApJ*, 668, 417-429 (2007).
60. Fragile, P. C., Lindner, C. C., Anninos, P., Salmonson, J. D., "Application of the Cubed-Sphere Grid to Tilted Black Hole Accretion Disks", *ApJ*, 691, 482F (2009).
61. First, F., Nowak, M. A., Tomsick, J. A., et al., "THE COMPLEX ACCRETION GEOMETRY OF GX 339?4 AS SEEN BY *NuSTAR* AND *SWIFT*", *ApJ*, 808, 122 (2015).
62. Gair, J. A., Vallisneri, M., Larson, S. L., Baker, J. G., "Testing General Relativity with Low-Frequency, Space-Based Gravitational-Wave Detectors", *Living Rev. Relativity*, 16, 7 (2013) [<http://www.livingreviews.org/lrr-2013-7>].
63. García, J. A., Dauser, T., Lohfink, A., "Improved Reflection Models of Black Hole Accretion Disks: Treating the Angular Distribution of X-Rays", *ApJ*, 782, 76G (2014).
64. García, J. A., Dauser, T., Reynolds, C. S., Kallman, T. R., McClintock, J. E., Wilms, J., Eikmann, W., "X-Ray Reflected Spectra from Accretion Disk Models. III. A Complete Grid of Ionized Reflection Calculations", *ApJ*, 768, 146 (2013).
65. García, J. A., Fabian, A. C., Kallman, T. R., Dauser, T., Parker, M. L., McClintock, J. E., Steiner, J. F., Wilms, J., "The effects of high density on the X-ray spectrum reflected from accretion discs around black holes", *MNRAS*, 462, 751-760 (2016).
66. García, J. A., Steiner, J. F., McClintock, J. E., Remillard, R. A., "X-RAY REFLECTION SPECTROSCOPY OF THE BLACK HOLE GX 339?4: EXPLORING THE HARD STATE WITH UNPRECEDENTED SENSITIVITY", *ApJ*, 813, 84 (2015).
67. Geroch, R., "Multipole Moments. II. Curved Space", *J. Math. Phys. (N.Y.)* 11, 2580 (1970).
68. Ghasemi-Nodehi, M., Bambi, C., "Constraining the Kerr parameters via x-ray reflection spectroscopy", *Phs. Rev. D*, 94j4062G (2016).
69. Gierliński, Marek, Maciołek-Niedźwiecki, A., Ebisawa, K., "Application of a relativistic accretion disc model to X-ray spectra of LMC X-1 and GRO J1655-40", *MNRAS*, 325, 1253G (2001).
70. Gilfanov, M., Merloni, A., "Observational Appearance of Black Holes in X-Ray Binaries and AGN", *Space Science Review*, 183, 121 (2014).
71. Glampedakis, K., Babak, S., "Mapping spacetimes with LISA: inspiral of a test body in a 'quasi-Kerr' field", *Classical and Quantum Gravity*, 23, 4167-4188 (2006).
72. Gonzalez, A. G., Wilkins, D. R., Gallo, L. C., "Probing the geometry and motion of AGN coronae through accretion disc emissivity profiles", *MNRAS*, 472, 1932G (2017).
73. Gou, L., McClintock, J. E., Liu, J., "A DETERMINATION OF THE SPIN OF THE BLACK HOLE PRIMARY IN LMC X-1", *ApJ*, 701, 1076-1090 (2009).
74. Gou, L., McClintock, J. E., Reid, M. J., et al., "The Extreme Spin of the Black Hole in Cygnus X-1", *ApJ*, 742, 85G (2011).
75. Gou, L., McClintock, J. E., Remillard, R., A., "CONFIRMATION VIA THE CONTINUUM-FITTING METHOD THAT THE SPIN OF THE BLACK HOLE IN CYGNUS X-1 IS EXTREME", 790, 29 (2014).
76. Greene, J., Bailyn, C. D., Orosz, J. A., "Optical and Infrared Photometry of the Microquasar GRO J1655-40 in Quiescence", *ApJ*, 554, 1290G (2001).

77. Hall, P., Sarrouh, G., Horne, K., “Non-Blackbody Disks Can Help Explain Inferred AGN Accretion Disk Sizes”, submitted to ApJ (2017) arXiv:1705.05467
78. Hansen, R. O., “Multipole moments of stationary spacetimes”, J. Math. Phys. (N.Y.), 15, 46 (1974).
79. Hoormann, J. K., Beheshtipour, B., Krawczynski, H., “Testing General Relativity’s No-Hair Theorem with X-Ray Observations of Black Holes”, Phys. Rev. D., 93, 044020 (2016).
80. Ingram, A., Done, C., Fragile, P. C., “Low-frequency quasi-periodic oscillations spectra and Lense-Thirring precession”, MNRAS, 397, L101-L105 (2009).
81. Ingram, A., Maccarone, T. J., Poutanen, J., Krawczynski, H., “Polarization Modulation from Lense-Thirring Precession in X-Ray Binaries”, ApJ, 807, 531 (2015).
82. Ingram, A., Maccarone, T. J., “An observational method for fast stochastic X-ray polarimetry timing”, MNRAS, 471, 4206-4217 (2017).
83. Israel, W., “Event Horizons in Static Vacuum Space-Times”, Phys. Rev., 164, 1776 (1967); Israel, W., “Event horizons in static electrovac space-times”, Comm. Math. Phys., 8, 245 (1968); Carter, B., “Axisymmetric Black Hole Has Only Two Degrees of Freedom”, Phys. Rev. Lett., 26, 331 (1971); Carter, B., “Black Hole Equilibrium States”, In: “Les Houches 1972, Black Holes, Les Astres Occlus”, DeWitt, C., DeWitt, B. S. (eds.), Gordon and Breach, NY, 1 edition, p. 57-214 (1973); Hawking, S. W., “Gravitational Radiation from Colliding Black Holes”, Phys. Rev. Lett., 26, 1344-1346 (1971); Hawking, S. W., “Black Holes in General Relativity”, Comm. Math. Phys., 25, 152-166 (1972); Robinson, D.C., “Uniqueness of the Kerr Black Hole”, Phys. Rev. Lett., 34, 905-906 (1975); Mazur, P. O., “Proof of uniqueness of the Kerr-Newman black hole solution”, J. Phys. A: Math. Gen., 15, 3173-3180 (1982); Heusler, M., “Black Hole Uniqueness Theorems”, Cambridge University Press, Cambridge (1996); Chruściel, P. T., Lopes Costa, J., Heusler, M., Living Rev. Relativ. 15: 7 (2012). <https://link.springer.com/article/10.12942/lrr-2012-7>; Mazur, P. O., “Black Hole Uniqueness Theorems” (2009) [<http://adsabs.harvard.edu/abs/2001hep.th....1012M>]; Robinson, D. C., “Four decades of black hole uniqueness theorems”, In: “The Kerr Spacetime: Rotating Black Holes in General Relativity”, pp. 115-143, eds. D L Wiltshire, M Visser, S M Scott, (Cambridge University Press, 2009) [https://nms.kcl.ac.uk/david.robinson/web_page/blackholes.pdf].
84. Ivanov, P. B., Illarionov, A. F., “The oscillatory shape of the stationary twisted disc around a Kerr black hole”, MNRAS, 285, 394-402 (1997).
85. Jiang, Y. F., Davis, S. W., Stone, J., M., “IRON OPACITY BUMP CHANGES THE STABILITY AND STRUCTURE OF ACCRETION DISKS IN ACTIVE GALACTIC NUCLEI”, ApJ, 827, 10 (2016).
86. Jiang, Y.-F., et al., “Detection of Time Lags between Quasar Continuum Emission Bands Based On Pan-STARRS Light Curves”, ApJ, 836, 186 (2017).
87. Johannsen, T., Psaltis, D., “Metric for rapidly spinning black holes suitable for strong-field tests of the no-hair theorem”, Phys. Rev. D, 83, 124015 (2011).
88. Johannsen, T., “Regular black hole metric with three constants of motion”, Phys. Rev. D., 88, 044002 (2013).
89. Johannsen, T., Psaltis, D., “TESTING THE NO-HAIR THEOREM WITH OBSERVATIONS IN THE ELECTROMAGNETIC SPECTRUM. IV. RELATIVISTICALLY BROADENED IRON LINES”, ApJ, 773, 57J (2013).
90. Johannsen, T., “Systematic study of event horizons and pathologies of parametrically deformed Kerr spacetimes”, Phys. Rev. D., 87, 124017 (2013).
91. Johannsen, T., “PHOTON RINGS AROUND KERR AND KERR-LIKE BLACK HOLES”, ApJ, 777, 117 (2013).
92. Johannsen, T., “X-ray probes of black hole accretion disks for testing the no-hair theorem”, Phys. Rev. D, 90, 064002 (2014).
93. Johannsen, T., “Testing the no-hair theorem with observations of black holes in the electromagnetic spectrum”, Class. Quantum Grav., 33, 124001 (2016).
94. Kerr, R. P., “Gravitational Field of a Spinning Mass as an Example of Algebraically Special Metrics”, Phys. Rev. Lett., 11, 237 (1963).
95. Khargharia, J., Froning, C. S., Robinson, E. L., “NEAR-INFRARED SPECTROSCOPY OF LOW-MASS X-RAY BINARIES: ACCRETION DISK CONTAMINATION AND COMPACT OBJECT MASS DETERMINATION IN V404 Cyg AND Cen X-4”, ApJ, 716, 1105-1117 (2010).
96. Kislat, F., Beheshtipour, B., Dowkontt, P., et al., “Design of the Telescope Truss and Gondola for the Balloon-Borne X-ray Polarimeter X-Calibur”, JAI, 640003K (2017).
97. Kleihaus, B., Kunz, J., Radu, E., “Rotating Black Holes in Dilatonic Einstein-Gauss-Bonnet Theory”, Phys. Rev. Lett., 106, 151104 (2011).
98. Kolehmainen, M., Done, C., “Limits on spin determination from disc spectral fitting in GX 339-4”, MNRAS, 406, 2206-2212 (2010).
99. Kolehmainen, M., Done, C., Díaz Trigo, M., “Modelling the high-mass accretion rate spectra of GX 339-4: black hole spin from reflection?”, MNRAS, 416, 311-321 (2011).
100. Kong, L., Li, Z., Bambi, C., “CONSTRAINTS ON THE SPACETIME GEOMETRY AROUND 10 STELLAR-MASS BLACK HOLE CANDIDATES FROM THE DISK’S THERMAL SPECTRUM”, ApJ, 797, 78 (2014).
101. Konoplya, R., Rezzolla, L., Zhidenko, A., “General parametrization of axisymmetric black holes in metric theories of gravity”, Phys. Rev. D., 93, 064015 (2016).
102. Krawczynski, H., “Tests of General Relativity in the Strong-gravity Regime Based on X-Ray Spectropolarimetric Observations of Black Holes in X-Ray Binaries”, ApJ, 754, 133 (2012).
103. Krawczynski, H., Chartas, G., “Modeling of the Microlensed Fe K α Emission from the Quasar RX J1131-1231”, ApJ, 843, 118K (2017).
104. Krawczynski, H., Stern, D., Harrison, F. A., et al., “X-ray polarimetry with the Polarization Spectroscopic Telescope Array (PoSTAR)”, Aph, 75, 8K (2016).
105. Kulkarni, A. K., Penna, R. F., Shcherbakov, R. V., et al., “Measuring black hole spin by the continuum-fitting method: effect of deviations from the Novikov-Thorne disc model”, MNRAS, 414, 1183 (2011).
106. Kumar, S., Pringle, J. E., “Twisted accretion disks: the Bardeen-Petterson effect”, MNRAS, 213, 435-442 (1985).
107. Lense, J., Thirring, H., “Über die Einfluß der Eigenrotation der Zentralkörper auf die Bewegung der Planeten und Monde nach der Einsteinschen Gravitationstheorie”, Zeit. Phys. 19, 156-163 (1918).
108. Li, L.-X., Narayan, R., McClintock, J. E., et al., “Inferring the Inclination of a Black Hole Accretion Disk from Observations of its Polarized Continuum Radiation”, ApJ, 691, 847L (2009).
109. LIGO Scientific Collaboration and Virgo Collaboration, Fermi Gamma-ray Burst Monitor, and INTEGRAL, “Gravitational Waves and Gamma-Rays from a Binary Neutron

- Star Merger: GW170817 and GRB 170817A", *ApJL*, 848, L13 (2017).
110. Lubow, S. H., Ogilvie, G. I., Pringle, J. E., "The evolution of a warped disc around a Kerr black hole", *MNRAS*, 337, 706-712 (2002).
 111. Maccarone T. J., "On the misalignment of jets in microquasars", *MNRAS*, 336, 1371 (2002), "Erratum: On the misalignment of jets in microquasars", *MNRAS*, 446, 3162M (2015).
 112. MacLeod, C. L., Morgan, C. W., Mosquera, A., et al., "A Consistent Picture Emerges: A Compact X-Ray Continuum Emission Region in the Gravitationally Lensed Quasar SDSS J0924+0219", *ApJ*, 806, 258M (2015).
 113. Marin, F., Dovčiak, M., Muleri, F., Kislak, F. F., Krawczynski, H. S., "Predicting the X-ray polarization of type 2 Seyfert galaxies", *MNRAS*, 473, 1286M (2018).
 114. Marshall, M. D., Avara, M. J., McKinney, J. C., "Angular Momentum Transport in Thin Magnetically Arrested Disks" (2017), *arXiv:1709.10113*.
 115. Martin, R. G., Tout, C. A., Pringle, J. E., "Alignment time-scale of the microquasar GRO J1655-40", *MNRAS*, 387, 188 (2008).
 116. Matt, G., Perola, G. C., Piro, L., "The iron line and high energy bump as X-ray signatures of cold matter in Seyfert 1 galaxies", *A&A*, 247, 25 (1991).
 117. McClintock, J. E., Narayan, R., Steiner, J. F., "Black Hole Spin via Continuum Fitting and the Role of Spin in Powering Transient Jets", *Space Science Review*, 183, 295M (2014).
 118. McClintock, J. E., Shafee, R., Narayan, R., Remillard, R. A., Davis, S. W., Li, L.-X., "THE SPIN OF THE NEAR-EXTREME KERR BLACK HOLE GRS 1915+105", *ApJ*, 652, 518-539 (2006).
 119. Middleton, M., Done, C., Gierliński, M., Davis, S. W., "Black hole spin in GRS 1915+105", *MNRAS*, 373, 1004-1012 (2006).
 120. Miller, J. M., "Relativistic X-Ray Lines from the Inner Accretion Disks Around Black Holes", *Ann. Rev. Astron. Astrophys.*, 45, 441-79 (2007).
 121. Miller, J. M., Pooley, G. G., Fabian, A. C., et al., "ON THE ROLE OF THE ACCRETION DISK IN BLACK HOLE DISK-JET CONNECTIONS", *ApJ*, 757, 11 (2012).
 122. Miller, J. M., Parker, M. L., Fürst, F., et al., "NuSTAR SPECTROSCOPY OF GRS 1915+105: DISK REFLECTION, SPIN, AND CONNECTIONS TO JETS", *ApJL*, 775, L45 (2013).
 123. Miller, J. M., Reynolds, C. S., Fabian, A. C., Miniutti, G., Gallo, L. C., "Stellar-Mass Black Hole Spin Constraints from Disk Reflection and Continuum Modeling", *ApJ*, 697, 900M (2009).
 124. Mishra, B., Fragile, P. C., Johnson, L. C., Kluźniak, W., "Three-dimensional, global, radiative GRMHD simulations of a thermally unstable disc", *MNRAS*, 463, 3437M (2016).
 125. Morales Teixeira, D., Fragile, P. C., Zhuravlev, V. V., Ivanov, P. B., "CONSERVATIVE GRMHD SIMULATIONS OF MODERATELY THIN, TILTED ACCRETION DISKS", 796, 103 (2014).
 126. Morgan, C. W., Kochanek, C. S., Morgan, N. D., & Falco, E. E., "The Quasar Accretion Disk Size-Black Hole Mass Relation", *ApJ*, 712, 1129 (2010).
 127. Morgan, C. W., et al., "Further Evidence that Quasar X-Ray Emitting Regions are Compact: X-Ray and Optical Microlensing in the Lensed Quasar Q J0158-4325", *ApJ*, 756, 52 (2012).
 128. Mosquera, A. M., "The Structure of the X-Ray and Optical Emitting Regions of the Lensed Quasar Q 2237+0305", *ApJ*, 769, 53 (2013).
 129. Nandra, K., "ATHENA: The Advanced Telescope for High Energy Astrophysics", *The X-ray Universe 2011*, Berlin, Germany, 27-30 June 2011 (2011) [https://www.cosmos.esa.int/documents/332006/954767/Nandra_TopicK.pdf].
 130. Narayan, R., Zhu, Y., Psaltis, D., Sądowski, A., "HEROIC: 3D general relativistic radiative post-processor with comptonization for black hole accretion discs", *MNRAS*, 457, 608 (2016).
 131. Neustroev, V. V., Veledina, A., Poutanen, J., Zharikov, S. V., Tsygankov, S. S., Sjöberg, G., Kajava, J. J. E., "Spectroscopic evidence for a low-mass black hole in SWIFT J1753.5-0127", *MNRAS*, 445, 2424N (2014).
 132. Newman, E., Adamo, T., "Kerr-Newman metric", *Scholarpedia*, 9, 31791 (2014), [http://www.scholarpedia.org/article/Kerr-Newman_metric].
 133. Newman, E. T., Couch, E., Chinnapared, K., Exton, A., Prakash, A., and Torrence, R., "Metric of a Rotating, Charged Mass", *Journal of Mathematical Physics*, 6, 918 (1965).
 134. Noble, S. C., et al., "Radiative Efficiency and Thermal Spectrum of Accretion onto Schwarzschild Black Holes", *ApJ*, 743, 115 (2011).
 135. Novikov, I. D., Thorne, K. S., "Black Hole Equilibrium States", In: "Les Houches 1972, Black Holes, Les Astres Occlus", DeWitt, C., DeWitt, B. S. (eds.), Gordon and Breach, NY, 1 edition, p. 343-450 (1973).
 136. Orosz, J. A., McClintock, J. E., Remillard, R. A., Corbel, S., "Orbital Parameters for the Black Hole Binary XTE J1650-500", *ApJ*, 616, 376O (2004).
 137. Orosz, J. A., McClintock, J. E., Aufdenberg, J. P., Remillard, R. A., Reid, M. J., Narayan, R., Gou, L., "THE MASS OF THE BLACK HOLE IN CYGNUS X-1", *ApJ*, 742, 84O (2011).
 138. Page, D. N., Thorne, K. S., "Disk-Accretion onto a Black Hole. Time-Averaged Structure of Accretion Disk", *ApJ*, 191, 499 (1974).
 139. Pani, P., Macedo, C. F. B., Crispino, L. C. B., Cardoso, V., "Slowly rotating black holes in alternative theories of gravity", *Phys. Rev. D*, 84, 087501 (2011).
 140. Papaloizou, J. C. B., Lin, D. N. C., "On the dynamics of warped accretion disks", *ApJ*, 438, 841P (1995).
 141. Papaloizou, J. C. B., Pringle, J. E., "The time-dependence of non-planar accretion disks", *MNRAS*, 202, 1181-1194 (1983).
 142. Parker, M. L., Tomsick, J. A., Kennea, J. A., et al., "NuSTAR AND SWIFT OBSERVATIONS OF THE VERY HIGH STATE IN GX 339-4: WEIGHING THE BLACK HOLE WITH X-RAYS", *ApJ*, 821, L6 (2016).
 143. Penna, R. F., Sądowski, A., McKinney, J. C., "Thin-disc theory with a non-zero-torque boundary condition and comparisons with simulations", *MNRAS*, 420, 684-698 (2012).
 144. Poisson, E., Will, C. M., "Gravity: Newtonian, Post-Newtonian, Relativistic", 1st Edition, Cambridge University Press; 1 edition (2014).
 145. Psaltis, D., "Probes and Tests of Strong-Field Gravity with Observations in the Electromagnetic Spectrum", *Living Rev. Relativ.* 11: 9 (2008) [<https://doi.org/10.12942/lrr-2008-9>].
 146. Psaltis, D., Johannsen, T., "A Ray-tracing Algorithm for Spinning Compact Object Spacetimes with Arbitrary Quadrupole Moments. I. Quasi-Kerr Black Holes", *ApJ*, 745, 6 (2012).
 147. Remillard, R. A., McClintock, J. E., "X-Ray Properties of Black-Hole Binaries", *Ann. Rev. Astron. Astrophys.*, 44, 49R (2006).

148. Reid, M. J., McClintock, J. E., Narayan, R., Gou, L., Remillard, R. A., Orosz, J. A., "The Trigonometric Parallax of Cygnus X-1", *ApJ*, 742, 83R (2011).
149. Reid, M. J., McClintock, J. E., Steiner, J. F., Steeghs, D., Remillard, R. A., Dhawan, V., Narayan, R., "A PARALLAX DISTANCE TO THE MICROQUASAR GRS 1915+105 AND A REVISED ESTIMATE OF ITS BLACK HOLE MASS", *ApJ*, 796, 2 (2014).
150. Reis, R. C., Fabian, A. C., Ross, R. R., Miller, J. M., "Determining the spin of two stellar-mass black holes from disc reflection signatures", *MNRAS*, 395, 1257-1264 (2009).
151. Reis, R. C., Fabian, A. C., Ross, R. R., Miniutti, G., Miller, J. M., Reynolds, C., "A systematic look at the very high and low/hard state of GX 339-4: constraining the black hole spin with a new reflection model", *MNRAS*, 387, 1489-1498 (2008).
152. Reis, R. C., Miller, J. M., Reynolds, M. T., Fabian, A. C., Walton, D. J., "Suzaku Observation of the Black Hole Candidate Maxi J1836-194 in a Hard/Intermediate Spectral State", *ApJ*, 751, 34R (2012).
153. Reis, R. C., Reynolds, M. T., Miller, J. M., Walton, D. J., "Reflection From the Strong Gravity Regime in a $z = 0.658$ Gravitationally Lensed-Quasar", *Nature*, 507, 207 (2014).
154. Reynolds, C. S., Fabian, A. C., "Special relativistic effects on the strength of the fluorescent Kalpha iron line from black hole accretion discs", *MNRAS*, 290L, 1R (1997).
155. Risaliti, G., Harrison, F. A., Madsen, K. K., et al., "A rapidly spinning supermassive black hole at the centre of NGC 1365", *Nature*, 494, 449-451 (2013).
156. Ross, R. R., Fabian, A. C., "A comprehensive range of X-ray ionized-reflection models", *MNRAS*, 358, 211, (2005).
157. Russell, T. D., Soria, R., Motch, C., "The face-on disc of MAXI J1836-194", *MNRAS* 439, 1381-1389 (2014).
158. Ryan, F. D., "Gravitational waves from the inspiral of a compact object into a massive, axisymmetric body with arbitrary multipole moments", *Phs. Rev. D*, 52, 5707R (1995).
159. Ryan, B. R., Ressler, S. M., Dolence, J. C., Tchekhovskoy, A., Gammie, C., Quataert, E., "The Radiative Efficiency and Spectra of Slowly Accreting Black Holes from Two-temperature GRRMHD Simulations", *ApJ*, 844L, 24R (2017).
160. Sądowski, A.; Narayan, R., "Three-dimensional simulations of supercritical black hole accretion discs - luminosities, photon trapping and variability", *MNRAS*, 456, 3929 (2016).
161. Schnittman, J. D., Homan, J., Miller, J. M., "A Precessing Ring Model for Low-Frequency Quasi-periodic Oscillations", *ApJ*, 642, 420S (2006).
162. Schnittman, J. D., Krolik, J. H., "X-ray Polarization from Accreting Black Holes: The Thermal State", *ApJ*, 701, 1175S (2009).
163. Schnittman, J. D., Krolik, J. H., "X-ray Polarization from Accreting Black Holes: Coronal Emission", *ApJ*, 712, 908S (2010).
164. Schnittman, J. D., Angelini, L.; Baring, M., et al., "X-ray Polarization from Black Holes: GEMS Scientific White Paper" (2013) [arXiv1301.1957S].
165. Schnittman, J. D., Krolik, J. H., Noble, S. C., "X-Ray Spectra from Magnetohydrodynamic Simulations of Accreting Black Holes", *ApJ*, 769, 156 (2013).
166. Shakura, N. I., Sunyaev, R. A., "Black Holes in Binary Systems: Observational Appearance", *A&A*, 24, 337-355 (1973).
167. Shafee, R., McClintock, J. E., Narayan, R., Davis, S. W., Li, L.-X., Remillard, R. A., "ESTIMATING THE SPIN OF STELLAR-MASS BLACK HOLES BY SPECTRAL FITTING OF THE X-RAY CONTINUUM", *ApJL*, 636, L113 (2006).
168. Shimura, T., Takahara, F., "On the spectral hardening factor of the X-ray emission from accretion disks in black hole candidates", *ApJ*, 445, 780-788 (1995).
169. Sotiriou, T. P., Limerati, S., "THEORY OF GRAVITATION THEORIES: A NO-PROGRESS REPORT", *International Journal of Modern Physics D*, Vol. 17, Nos. 3 & 4, 399-423, (2008).
170. Stefanov, I. Z., "Confronting models for the high-frequency QPOs with Lense-Thirring precession", *MNRAS*, 444, 2178S (2014).
171. Steiner, J. F., McClintock, J. E., "MODELING THE JET KINEMATICS OF THE BLACK HOLE MICROQUASAR XTE J1550-564: A CONSTRAINT ON SPIN-ORBIT ALIGNMENT", *ApJ*, 745, 136 (2012).
172. Steiner, J. F., McClintock, J. E., Orosz, J. A., Remillard, R. A., Bailyn, C. D., Kolehmainen, M., Straub, O., "THE LOW-SPIN BLACK HOLE IN LMC X-3", *ApJ*, 793, 29 (2014).
173. Steiner, J. F., Reis, R. C., Fabian, A. C., et al., "A broad iron line in LMC X-1", *MNRAS*, 427, 2552-2561 (2012).
174. Steiner, J. F., Reis, R. C., McClintock, J. E., et al., "The spin of the black hole microquasar XTE J1550-564 via the continuum-fitting and Fe-line methods", *MNRAS*, 416, 941 (2011).
175. Stella, L., Vietri, M., "Lense-Thirring Precession and Quasi-periodic Oscillations in Low-Mass X-Ray Binaries", *ApJ*, 492L, 59S (1998).
176. Stella, L., Vietri, M., Morsink, S. M., "Correlations in the Quasi-periodic Oscillation Frequencies of Low-Mass X-Ray Binaries and the Relativistic Precession Model", *ApJ*, 524L, 63S (1999).
177. Shakura, N. I., Sunyaev, R. A., "Black holes in binary systems. Observational appearance", *A&A*, 24, 337 - 355 (1973).
178. Teukolsky, S. A., "The Kerr metric", *Class. Quantum Grav.*, 32, 124006 (2015).
179. Thornburg, J., "Event and Apparent Horizon Finders for 3 + 1 Numerical Relativity", *Living Rev. Relativ.* 10:3 (2007) [<http://www.livingreviews.org/lrr-2007-3>].
180. Thorne, K. S., Will, C. M., "Theoretical Frameworks for Testing Relativistic Gravity. I. Foundations", *ApJ*, 163, 595T (1971).
181. Thorne, K. S., Price, R. H., MacDonald, D. A., "Black Holes, The Membrane Paradigm", Yale University Press, New Haven and London (1986).
182. Tomsick, J. A., Nowak, M. A., Parker, M., et al., "THE REFLECTION COMPONENT FROM CYGNUS X-1 IN THE SOFT STATE MEASURED BY NuSTAR AND SUZAKU" *ApJ*, 780, 78 (2014).
183. Tomsick, J. A., Parker, M. L., García, J. A., et al., "Alternative Explanations for Extreme Supersolar Iron Abundances Inferred from the Energy Spectrum of Cygnus X-1", *ApJ*, 855, 3 (2018).
184. Uttley, P., Cackett, E. M., Fabian, A. C., Kara, E., Wilkins, D. R., "X-ray reverberation around accreting black holes", *Astronomy and Astrophysics Review*, 22, 72 (2014).
185. Veledina, A., Poutanen, J., Ingram, A., "A Unified Lense-Thirring Precession Model for Optical and X-Ray Quasi-periodic Oscillations in Black Hole Binaries", *ApJ*, 778, 165V (2013).
186. van der Klis, M., "Rapid X-ray Variability", In: Compact stellar X-ray sources. Edited by Walter Lewin & Michiel van der Klis. Cambridge Astrophysics Series, No. 39. Cambridge, UK: Cambridge University

- Press, ISBN 978-0-521-82659-4, ISBN 0-521-82659-4, DOI: 10.2277/0521826594, p. 39 - 112 (2006).
187. Vigeland, S., Yunes, N., Stein, L. C., “Bumpy black holes in alternative theories of gravity”, *PhRvD*, 83j4027V (2011).
 188. Walton, D. J., Reis, R. C., Cackett, E. M., Fabian, A. C., Miller, J. M., “The similarity of broad iron lines in X-ray binaries and active galactic nuclei”, *MNRAS*, 422, 2510W (2012).
 189. Walton, D. J., Tomsick, J. A., Madsen, K. K., et al., “The Soft State of Cygnus X-1 Observed with NuSTAR: A Variable Corona and a Stable Inner Disk”, *ApJ*, 826, 87 (2016).
 190. Walton, D. J., Mooley, K., King, A. L., et al., “Living on a Flare: Relativistic Reflection in V404 Cyg Observed by NuSTAR during Its Summer 2015 Outburst”, *ApJ*, 839, 110W (2017).
 191. Weisskopf, M. C., Ramsey, B., O’Dell, S., et al., “The Imaging X-ray Polarimetry Explorer (IXPE)”, *SPIE*, 9905E, 17W (2016).
 192. Will, C., “The Confrontation between General Relativity and Experiment”, *Living Rev. Relativ.* 17: 4 (2014) [<https://doi.org/10.12942/lrr-2014-4>].
 193. Wilms, Jörn; Reynolds, C. S., Begelman, M. C., Reeves, J., Molendi, S., Staubert, R., Kendziorra, E., “XMM-EPIC observation of MCG-6-30-15: direct evidence for the extraction of energy from a spinning black hole?”, *MNRAS*, 328, 27 (2001).
 194. Wilkins, D. C., “Bound Geodesics in the Kerr Metric”, *Phys. Rev. D.*, 5, 814 (1974).
 195. Wilson-Hodge, C. A., Ray, P. S., Gendreau, K., “STROBE-X: X-ray Timing and Spectroscopy on Dynamical Timescales from Microseconds to Years”, *Res. in Physics*, 7, 3704W (2017).
 196. Yunes, N., Siemens, S., “Gravitational-Wave Tests of General Relativity with Ground-Based Detectors and Pulsar-Timing Arrays”, *Living Rev. Relativity*, 16, 9 (2013) [<http://www.livingreviews.org/lrr-2013-9>].
 197. Zhang, S.-N., “Black hole binaries and microquasars”, *FrPhy*, 8, 630Z (2013).
 198. Zhang, S.-N., Cui, Wei, Chen, Wan, “Black Hole Spin in X-Ray Binaries: Observational Consequences”, *ApJ*, 482L, 155Z (1997).
 199. Zhang, S.-N., Feroci, M., Santangelo, A., “eXTP: enhanced X-ray Timing and Polarimetry Mission”, *Proc. of SPIE*, 9905, 99051Q-1 (2016).
 200. Zhu, Y., Davis, S. W., Narayan, R., et al., “The eye of the storm: light from the inner plunging region of black hole accretion discs”, *MNRAS*, 424, 2504 (2012).
 201. Zhuravlev, V. V., Ivanov, P. B., “A fully relativistic twisted disc around a slowly rotating Kerr black hole: derivation of dynamical equations and the shape of stationary configurations”, *MNRAS*, 415, 2122-2144 (2011).
 202. Zhuravlev, V. V., Ivanov, P. B., Fragile, P. C., Morales Teixeira, D., “NO EVIDENCE FOR BARDEEN-PETTERSON ALIGNMENT IN GRMHD SIMULATIONS AND SEMI-ANALYTIC MODELS OF MODERATELY THIN, PROGRADE, TILTED ACCRETION DISKS”, *ApJ*, 796, 104 (2014).